The Pliensbachian-Toarcian paleoclimate transition: New insights from organic geochemistry and C, H, N isotopes in a continental section from Central Asia

Romain Tramoy, Johann Schnyder, T.T. Nguyen Tu, J. Yans, Jérémy Jacob, M. Sebilo, S. Derenne, M. Philippe, A. Huguet, D. Pons, et al.

The Pliensbachian-Toarcian paleoclimate transition: New insights from organic geochemistry and C, H, N isotopes in a continental section from Central Asia

R. Tramoy[a*], J. Schnyder[a], T. T. Nguyen Tu[b], J. Yans[c], J. Jacob[d], M. Sebilo[e], S. Derenne[b], M. Philippe[f], A. Huguet[b], D. Pons[g] and F. Baudin[a]

[a]*Sorbonne Universités, UPMC Univ Paris 06, CNRS, Institut des Sciences de la Terre de Paris (iSTeP), 4 place Jussieu, 75005 Paris, France.*

[b]*Sorbonne Universités, UPMC Univ Paris 06, CNRS, EPHE, UMR7619, Milieux Environnementaux, Transferts et Interactions dans les Sols (METIS), 4 place Jussieu, 75005 Paris, France.*

[c]*Université de Namur, Department of Geology, NaGRIDD, 61 rue de Bruxelles, 5000 Namur, Belgium.*

[d]*Institut des Sciences de la Terre d'Orléans, UMR 7327 CNRS-Université d'Orléans-BRGM, 1A rue de la Férollerie, 45000 Orléans, France.*

[e]*Sorbonne Universités, UPMC Univ Paris 06, CNRS, Institute of Ecology and Environmental Sciences (IEES), 4 place Jussieu 75005 Paris, France.*

[f]*Université Lyon 1, UMR 5026, CNRS, Campus de la Doua, Darwin A, F69622 Villeurbanne cedex, France.*

[g]*Sorbonne-Universités, UPMC Univ Paris 06, CNRS, MNHN, Centre de Recherche sur la Paléobiodiversité et les Paléoenvironnements (CR2P), 4 place Jussieu 75005 Paris, France.*

*Corresponding author: Romain Tramoy, phone: +33 6 76 28 08 38; e-mail: romain.tramoy@gmail.com

Highlights

- ⇨ Well-preserved Jurassic δ^2H signal of *n*-alkanes enables paleoclimatic interpretations.
- ⇨ Oldest ever glycerol dialkyl glycerol tetraethers temperatures are reconstructed.
- ⇨ Humid/cool temperate Late Pliensbachian, associated with high seasonality.
- ⇨ Slightly less humid/warmer conditions in the Early Toarcian.
- ⇨ No drastic changes recorded by the $\delta^{15}N_{org}$ values.

Abstract

The Taskomirsay section (South Kazakhstan) is a unique Pliensbachian-Toarcian sequence of lignites, clayey layers and silty-sandstones deposited in a fluvial/lacustrine environment with nearby swampy areas. This period, characterized by a drastic climate change, has been particularly studied in Western Tethyan marine environments, whereas very few studies focused on continental settings. Paleoflora analyses, associated with a multi-isotope approach, based on well-preserved Type-III bulk organic nitrogen isotopes ($\delta^{15}N_{org}$) and hydrogen isotopic composition (δ^2H) of *n*-alkanes, were developed to document paleoclimatic changes in the area. Sporomorph associations and fossil woods revealed a globally warm- to cool-temperate climate – characterized by *Xenoxylon*, a conifer morphogenus biogeographically related to cool/humid settings – apart from slightly less humid and warmer conditions in the early Toarcian. Warmer conditions are supported by reconstructed Mean Annual Air Temperatures (MAATs), based on the first branched glycerol dialkyl glycerol tetraethers (brGDGTs) ever recorded in the Early Jurassic. Nevertheless, no drastic changes were recorded in the $\delta^{15}N_{org}$ values; its signal being attributed to tenuous equilibrium between water- and nutrient-availability via intense N-recycling. Based on *n*-alkane distributions, sources of organic matter were separated in two pools: (i) a purely

terrestrial (*n*-C_{27}) and (ii) an "aquatic" pool (*n*-C_{23}) constituted of vegetation that thrived under almost permanent water supply. The *n*-alkane δ^2H values (−248 to −151 ‰) as well as their amounts and average chain lengths (ACL) are in agreement with cool-temperate conditions in the Pliensbachian and less humid/warmer conditions in the early Toarcian. The isotopic difference between δ^2H values of *n*-C_{27} and *n*-C_{23} ($\Delta^2H_{ter\text{-}aq}$) suggests enhanced seasonality during the Pliensbachian-Toarcian transition and low seasonality in the early Toarcian, in agreement with temperate climate-regime. Finally, contrasted response to paleoclimate changes between markers suggests different spatial integration of those proxies. The role of sea-level variations for δ^2H values might also resolve this contrasted response.

Keywords

n-Alkanes, δ^2H, $\delta^{15}N_{org}$, *Xenoxylon*, brGDGT

1. Introduction

Major paleoenvironmental changes have been documented during the Early Jurassic and particularly in Western Tethyan marine sections during the Pliensbachian-Toarcian transition (Jenkyns, 1988; Bassoullet and Baudin, 1994; Bailey et al., 2003; Morard et al., 2003; Rosales et al., 2004; Hesselbo et al., 2007; Suan et al., 2010; Hermoso et al., 2012; Korte et al., 2015). During the late Pliensbachian, a 5°—6 °C decrease in sea surface temperatures has been evidenced by $\delta^{18}O$ and Mg/Ca of carbonates, possibly related to ice sheet development at high latitudes (Bailey et al., 2003; Rosales et al., 2004; van de Schootbrugge et al., 2005; Suan et al., 2010), and a sea level drop (Hallam, 1967; Hesselbo and Jenkyns, 1998). Then, a period of drastic warming (~8 °C) has been recorded in sea-surface temperatures during the early Toarcian (Bailey et al., 2003; Rosales et al., 2004; Suan et al., 2010), associated with a sea level rise (Hallam, 1967; Hesselbo and Jenkyns, 1998). The global scale of

paleoenvironmental disturbances during the Pliensbachian-Toarcian transition was confirmed by studies on sites located outside Europe in (i) the Neuquén Basin in Argentina (Al-Suwaidi et al., 2010), (ii) the High Atlas, Morocco (Bodin et al., 2010), (iii) the Qaidam Basin, Northwest China (Wang et al., 2005), (iv) the Clarence-Moreton Basin, Eastern Australia (Jansson et al., 2008) and (v) the Arctic (Suan et al., 2011). However, only few studies have focused on non-marine records (Wang et al., 2005; Jansson et al., 2008), mainly because well-dated terrestrial records for the Early Jurassic are much less common than marine ones (Sobel, 1999).

The Taskomirsay section (South Kazakhstan, Central Asia) is made of non-marine, coal-rich sediments that encompass the Pliensbachian-Toarcian transition (Schnyder et al., accepted). This section is a unique target for paleoclimatic reconstructions prior to and during the Pliensbachian-Toarcian transition in a continental setting. A multi-proxy approach was developed to document paleoclimatic changes in the area based on (i) palynological and paleobotanical records, (ii) bulk geochemistry (Rock-Eval and $\delta^{15}N_{org}$), (iii) *n*-alkane distribution and their hydrogen isotopic composition ($\delta^{2}H$), and (iv) branched glycerol dialkyl glycerol tetraethers (brGDGTs).

Palynological records (Schnyder et al., accepted), combined with paleobotanical evidences can help to decipher paleoclimatic background as some wood taxa are paleoecologically well constrained (Philippe and Thévenard, 1996; Philippe and Tchoumatchenco, 2008; Philippe et al., 2013; Oh et al., 2015). Recently, $\delta^{15}N_{org}$ measured in lignites and clayey layers was used to indicate wet/dry cycles during the Paleocene-Eocene transition (Storme et al., 2012) and the Eocene-Oligocene transition (Tramoy et al., 2016). Early studies indeed showed that $\delta^{15}N_{org}$ values were positively correlated to temperature and negatively to precipitation in Quaternary and modern plants (Austin and Vitousek, 1998; Handley et al., 1999; Amundson et al., 2003; Swap et al., 2004; Liu and Wang, 2008).

Considering the potential of $\delta^{15}N_{org}$ as a paleoclimatic marker for pre-Quaternary sediments (Storme et al., 2012; Tramoy et al., 2016), it will be tested in the Early Jurassic of the Taskomirsay sequence. Similarly, compound-specific $\delta^{2}H$ values are often used as a paleohydrological proxy (Sachse et al., 2012; Sessions, 2016). Major calibration efforts during the last decade allowed improving their use for paleoclimatic reconstructions in the Quaternary (e.g., Hou et al., 2006; Jacob et al., 2007; Mügler et al., 2008; Aichner et al., 2010), but also in the Cenozoic (Andersen et al., 2001; Pagani et al., 2006; Garel et al., 2013), and even in the Paleozoic (Dawson et al., 2004; Izart et al., 2012). However, to the best of our knowledge, compound-specific $\delta^{2}H$ values have only been scarcely used in Mesozoic sediments and not for paleoclimatic purpose (Radke et al., 2005). Yet, the $\delta^{2}H$ of *n*-alkanes preserved in ancient sediments has great potential because *n*-alkanes are much less prone to diagenetic effect than other compounds, because H is strongly bound to C and thus alkanes retain their original hydrogen isotopic composition (Yang and Huang, 2003; Izart et al., 2012; Sessions, 2016). During the last decade, proxies based on branched bacterial membrane lipids (brGDGTs; Schouten et al., 2013), have been developed to reconstruct Mean Annual Air Temperatures in terrestrial settings (MAAT; Weijers et al., 2007; Peterse et al., 2012; Coffinet et al., 2014) and their use for ancient sediments deserves evaluation.

The aim of the present study was to assess the paleoclimatic conditions during the Pliensbachian-Toarcian transition in the sedimentary succession of Taskomirsay using multi-proxy analyses: paleobotany, $\delta^{15}N_{org}$, *n*-alkane distributions and $\delta^{2}H$ values, and, although restricted to a selected set of samples, brGDGTs.

2. Material and methods

2.1. Taskomirsay section

The Taskomirsay section is located in the Karatau (Leontiev Graben), South Kazakhstan, which is one of the numerous continental basins, in central Asia, aligned along the North Tethyan-paleomargin (Fig. 1). These basins were formed by collisions between Eurasia and several blocks (Tarim, Tian Shan and Pamir Kunlun) in a transtensional/transpressional context between the Late Triassic and the Early Jurassic (Sobel, 1999). During the Early Jurassic, the paleolatitudinal position of the Karatau basin was estimated to 36° ± 8° N, based on paleomagnetic reconstructions (B. Vrielynck, pers. com. 2014), in agreement with paleofloral assemblages (40° N; Kirichkova and Doludenko, 1996), which is very close to present latitudes (Fig. 1). Thick piles of terrestrial sediments were deposited thanks to the coexisting high tectonic subsidence.

The study section is 53.5 m thick (0 m represents the base of the section) and shows 6 organic-rich sedimentary cycles (Fig. 2; Schnyder et al., accepted). Each cycle exhibits lignite beds (noted LB1 to LB6) overlaid by non-laminated clayey layers and silty-sandstone showing root and trunk surfaces at their top. The succession of lignites, clayey layers and silty-sandstones suggests a meandering river system, in which developed oxbow lakes and peat deposits thanks to the lateral migration of the river system. At the top of the section, a more open and less marginal lacustrine environment under storm influence is deduced from *Botryococcus*, clay/silt alternations and hummocky cross-beddings (HCS) (Schnyder et al., accepted). Wood fragments are frequent along the section and are particularly concentrated in three surfaces labeled TP1, TP2 and TP3 (Fig. 2). Macroscopically, they exhibit an excellent morphological preservation and are found in the tops and insides of silty-sandstones, and always in vertical position, suggesting *in situ* trunks or roots (Schnyder et al., accepted). These sedimentological features are in agreement with peaty/swampy forests in lowland

terrains and trees in sandy river banks and/or in upland forests, as might be expected from the paleoclimatic latitudinal patterns during the Early Jurassic, with warm to cool-temperate conditions prevailing from mid to high boreal latitudes (Miao et al., 1989; Rees et al., 2000; Wang et al., 2005).

Despite the common difficulty to date such continental settings, the Pliensbachian-Toarcian transition was identified between ~26 m and ~35 m, based on sporomorph associations and organic carbon isotopes ($\delta^{13}C_{org}$; Schnyder et al., accepted). The section was thus dated no younger than the early Toarcian and no older than the mid-Pliensbachian.

2.2. Analytical methods

2.2.1. Fossil wood analyses

Fossil wood samples were studied with collodion micro-casting, following a method described in Marynowski et al. (2013). Despite their good macroscopic morphological preservation, woody axes were revealed to be microscopically degraded by both bacterial and fungal rots. This condition is consistent with a relatively slow burial history, before diagenesis stopped biological decay. As a consequence, only one specimen was preserved enough for specific identification, although the others did not display significantly different features that could suggest a different systematic position. The wood specimen was identified at a generic level from the Philippe and Bamford (2008) key and at a species level with the Philippe et al. (2013) key.

2.2.2. Bulk organic analyses

Total organic carbon (TOC) values were obtained for 100 samples, sampled regularly along the study section, using a Leco automatic carbon analyzer (IR-212) that gives more reliable TOC values for samples containing large amounts of terrestrial OM than Rock-Eval

pyrolysis (Espitalié et al., 1985). A total of 88 samples, including 3 replicates, were analyzed by Rock-Eval pyrolysis using a Rock-Eval 6. For this study, the following Rock-Eval parameters were used: (i) Hydrogen Index (HI, mg HC/g TOC), which is the amount of products released during pyrolysis normalized to TOC values; (ii) Oxygen Index (OI, mg CO_2/g TOC), calculated from the amounts of CO and CO_2 released during pyrolysis, which represents the oxygen content of the OM; and (iii) T_{max}, which is the temperature of the pyrolysis oven recorded at the maximum of HC production (Espitalié et al., 1985). After Rock-Eval pyrolysis, a few samples were suspected to contain siderite that compromised measurements of the Rock-Eval parameters, especially for OI values. This suspicion was supported by very low dissolution rate of carbonates in 6N HCl. Concerned samples were removed from the dataset. In addition, samples with low S2 peak values (S2 <0.3) – leading to misestimation of HI values, were also removed. In total, 29 samples were removed from the dataset and will not be discussed further.

2.2.3. Bulk organic nitrogen isotopes ($\delta^{15}N_{org}$)

A total of 52 samples were analyzed for $\delta^{15}N_{org}$. Only samples with TOC values >1 wt. % were selected, because nitrogen content in Taskomirsay sediments is usually very low. Because inorganic nitrogen (N_{bnd}) is strongly bound to clay minerals as ammonium (Müller, 1977), it is easier to remove organic nitrogen (N_{org}) and recalculate the $\delta^{15}N_{org}$ by mass-balance, knowing total nitrogen (N_{tot}), N_{bnd} and their respective isotopic signatures $\delta^{15}N_{tot}$ and $\delta^{15}N_{bnd}$ (Storme et al., 2012). N_{tot} and $\delta^{15}N_{tot}$ were measured on powdered/decalcified samples, whereas N_{bnd} and $\delta^{15}N_{bnd}$ were measured on subsamples that were treated with KOBr-KOH solution (2 mol/l) to eliminate the N_{org} (Silva and Bremner, 1966; Schubert and Calvert, 2001). The solution consisted of 6 ml pure bromine added at 0.5 mL/min to 200 ml of 2M KOH cooled with ice. Between 500 to 1000 mg of subsamples were immersed in 20

ml of the KOBr-KOH solution with magnetic stirring. After 2 hours, 60 ml of distilled water was added to each subsample before being boiled in an oil-bath at ~200 °C for at least 5 min. With this treatment, organic nitrogen is liberated in ammonium form and stays in solution. The mixture was washed the next day by repetitive centrifugation (2x; 4000 rpm; 1.5 min) with 0.5 M of KCl to remove the released ammonium. Potassium added to the solution process prevents the adsorption by clay minerals of the ammonium released during the previous oxidation. Then, subsamples were washed again with distilled water to remove nitrogen complex salts from the solution. Samples were finally dried and powdered again for isotope analyses.

N_{tot}, N_{bnd} of samples and their respective isotopic signature $\delta^{15}N_{tot}$ and $\delta^{15}N_{bnd}$ were determined by mass spectrometry using a Thermo Scientific Delta V plus mass spectrometer connected to a ConFlo IV dilution system, coupled with a Flash 2000 analyzer for elemental analyses. The analytical accuracy and precision of the system were monitored using tyrosine ($\delta^{15}N$ = 10.01 ‰) as an internal laboratory standard, that was calibrated on international standards IAEA-N-1 ($\delta^{15}N$ = 0.4 ‰), IAEA-N-2 ($\delta^{15}N$ = 20.3 ‰) and IAEA-NO-3 ($\delta^{15}N$ = 4.7 ‰). Isotopic values were then expressed relative to the international N_2 air reference. The overall precision was better than 0.2 ‰ above 40 µg of nitrogen and 0.3 ‰ below this amount. Replicate analyses led to a mean standard deviation better than 0.1 ‰ for $\delta^{15}N$ values and better than 0.001 % for the nitrogen content. For isotopic values measured with nitrogen amount above 40 µg, the replicate standard deviation was applied. For those measured below this amount, the standard deviation based on tyrosine (0.3 ‰) was applied, even if the standard deviation based on replicates was lower.

2.2.4. Lipid extraction

Lipid extractions were performed on 11 lignites, 2 trunk/root-like samples, and 12 clayey layers. Samples were extracted with an accelerated solvent extractor (ASE 100, Dionex^{TM}), using a dichloromethane (DCM):methanol (MeOH) (2:1, v:v) mixture. A 34 mL cell was used with the following extraction protocol: temperature at 60 °C, pressure at 10^6 Pa, one static time during 20 min, 100 % flush and 100 s purge, all repeated 3 times. The lipid extract was then concentrated under vacuum and further evaporated under a smooth nitrogen flow to avoid loss of volatile molecules. The total lipid extracts (TLE) were then weighed, dissolved in heptane and separated on alumina solid phase extraction columns into an apolar and a polar fraction. The apolar fraction was eluted with heptane:DCM (99:1, v:v) and the polar fraction was eluted with DCM:MeOH (2:1, v:v). C_{12}-alkane was added as an internal standard before analysis by gas chromatography-mass spectrometry (GC-MS) for identification and quantification purposes. *n*-Alkane content, their Carbon Preference Index (CPI) and average chain length (ACL) were calculated as follows, over the range C_{21}-C_{35}:

n-alkane content = $\Sigma[C_i]$ (1)

$$CPI = \frac{1}{2} \times \left(\frac{\Sigma[C_{odd\,(21-35)}]}{\Sigma[C_{even\,(20-34)}]}\right) + \frac{1}{2} \times \left(\frac{\Sigma[C_{odd\,(21-35)}]}{\Sigma[C_{even\,(22-36)}]}\right) \quad (2)$$

$$\text{ACL} = \sum(C_i \times [C_i])/[C_i] \quad (3)$$

where $[C_i]$ is the concentration of the odd *n*-alkanes (µg/g TOC) with carbon number C_i.

Apolar fractions were further eluted with heptane on silica gel-type silica columns in order to purify the *n*-alkane fraction before δ^2H analysis by gas chromatography-isotope ratio

mass spectrometry (GC-irMS). Silica was previously extracted with DCM, then activated at 120 °C for 24 h and finally deactivated with 5 wt. % H_2O.

2.2.5. LC-MS analysis

Polar fractions obtained after separation of the TLEs over alumina columns were rotary evaporated, re-dissolved in 1 ml heptane and centrifuged using an Eppendorf Mini Spin centrifuge (1 min, 7000 rpm). The supernatant was collected and analyzed by high performance liquid chromatography-atmospheric pressure chemical ionization mass spectrometry (HPLC/APCI-MS). HPLC/APCI-MS analyses were performed with a Shimadzu LCMS-2020. GDGTs were analyzed using a procedure described in Huguet et al. (2013). MAAT were calculated using Weijers et al. (2007) and Peterse et al. (2012) calibrations, based on MBT and CBT indices as described in Coffinet et al. (2014).

2.2.6. GC-MS analysis

GC-MS analyses were performed on an Agilent 6890N gas chromatograph coupled with an Agilent 5973 Mass Selective Detector mass-spectrometer. The GC was fitted with a Restek RTX-5Sil-MS column (30 m × 0.25 mm i.d., 0.5 µm film thickness) under constant helium flow of 1 ml/min. Samples were dissolved in heptane and 1 µl injected in splitless mode with the injector temperature set at 320 °C. GC operating conditions were as follow: initial temperature hold at 80 °C for 30 s, then increased from 80 to 100 °C at 10 °C/min and from 100 to 320 °C at 4 °C/min with a final isothermal hold at 320 °C for 20 min. The mass spectrometer was operated in the electron ionization (EI) mode at 70 eV ionization energy and scanned from 35 to 800 Da. Biomarkers were identified based on mass spectra and retention times. Quantification was performed thanks to the peak area in Total Ion Current

(TIC) of each identified molecule. The peak areas were then normalized to the peak area of the internal standard C_{12}-alkane, measured on the TIC and then normalized to the total organic carbon (TOC) of the sample.

2.2.7. GC-irMS analysis (δ^2H)

The hydrogen isotopic composition of *n*-alkanes (δ^2H) was determined by GC-irMS using a Trace GC chromatograph equipped with a Triplus autosampler, connected to a GC-Isolink pyrolysis interface, a ConFlo IV dilution system coupled to a DeltaV Advantage isotope ratio mass spectrometer, all from ThermoElectron (Bremen, Germany). A mixture of *n*-alkanes (*n*-C_{16} to *n*-C_{30}, Arndt Schimmelmann, Indiana University, Bloomington, IN, USA) was analyzed before and after each set of 5 injections, allowing monitoring the precision and accuracy of the system. The overall precision for the *n*-alkane standard δ^2H values was better than 6 ‰ and were in good agreement with those measured off line. H_2 gas with known isotopic composition was used as an internal reference and δ^2H values of samples were normalized to the VSMOW international isotopic scale by using the standard *n*-alkane mixture. The mean precision (standard deviation) for triplicate analyses was better than 6 ‰ for δ^2H values of the C_{17} to C_{35} *n*-alkanes and of pristane, and better than 7 ‰ for phytane. The H_3^+ factor was calculated prior to analyses and was consistently below 3 ppm V^{-1}. Because of the low amount of biomarkers in some samples, only 18 samples could be analyzed for δ^2H out of 25 lipid extracts. Among the 18 samples, it was not possible to measure accurately the whole range of *n*-alkanes for all samples, depending on their respective concentration.

3. Results

3.1. Fossil woods

Many pieces of fossil woods are present along the section, although only one sample was positively identified as *Xenoxylon fuxinense* Ding in the TP3 trunk surface. The other samples (trunk surfaces 1, 2 and 3) did not seem to differ. However, their preservation state was too poor for safe identification. *X. fuxinense* is a secondary xylem documented from the Later Liassic (Negoya Fm.) of the Kuruma Group, Japan, to the Early Cretaceous (Aptian-Albian, Fuxin Fm.) of Liaoning, China. It is an Asian endemic taxon usually restricted to relatively high paleolatitudes (Philippe and Thévenard, 1996; Philippe et al., 2013).

3.2. Bulk geochemistry

Exhaustive TOC values and Rock-Eval data are available in supplementary data. TOC values range from 38.7 to 75.8 wt. % in lignites, from 0 to 24.4 wt. % in clayey layers and from 0 to 0.9 wt. % in silty-sandstones. Except for one coalified root/trunk, T_{max} values are always below 440 °C (424 °C in average). In lignites, HI values range from 38 to 217 mg HC/g TOC (128 mg HC/g on average) and OI values range from 19 to 80 mg CO_2/g TOC (35 mg CO_2/g TOC on average). In clayey layers, HI values range from 29 to 136 mg HC/g TOC (74 mg HC/g on average) and OI values range from 19 to 165 mg CO_2/g TOC (52 mg CO_2/g TOC on average). In an HI-OI diagram, the Taskomirsay samples plot in the Type-III zone (Fig. 3), suggesting an OM dominated by terrestrial plants (Espitalié et al., 1985).

Total nitrogen contents range between 0.05 and 1.48 wt. % (Table 1). Considering high TOC values (>40 %) in lignites and the very low amount of clay in this lithology, we assume that N_{tot} is almost equal to N_{org}. In a plot of $\%N_{tot}$ *vs* %TOC (Fig. 4), there is an intercept of

0.04 % N at 0 % TOC showing a significant fraction of inorganic N bound in clay minerals (Schubert and Calvert, 2001) for samples below 20 % of TOC (clayey layers), whereas there is a negligible intercept of 0.002 % N when considering $\%N_{org}$ *vs* %TOC. Thus, to calculate accurate atomic C/N ratios, we used N_{tot} for lignites and N_{org} for clayey layers. In Taskomirsay, C/N ratios range from 38 to 132 (Table 1).

3.3. Nitrogen isotopes

Together with the absence of clay – prone to adsorb inorganic nitrogen (Müller, 1977) – in lignites or coalified trunks, we argue for the use of the $\delta^{15}N_{tot}$ values as representatives of the $\delta^{15}N_{org}$ values. Indeed, Tramoy et al. (2016) have shown that $\delta^{15}N_{tot}$ values were driven by $\delta^{15}N_{org}$ values in Eocene-Oligocene terrestrial sediments. In Taskomirsay, the $\delta^{15}N_{tot}$ values range between 2.5 and 3.8 wt. ‰ (3.2 ‰ on average; Table 1 and Fig. 2). Except for one sample (TP3-224), $\delta^{15}N_{org}$ values of clay samples were almost equal to their $\delta^{15}N_{tot}$ values

3.4. Alkanes

n-Alkane amount range between 11 and 621 µg/g TOC (192 µg/g TOC on average; Table 2), except TP1-65 (clay) that yielded ~3300 µg/g TOC. It is noteworthy that the amount of *n*-alkanes decreases from the base of the section to the base of LB5 at 32.3 m, before it increases to the top. These trends are even more marked within lignite beds, with values gradually decreasing from LB1 to LB5 (315 µg/g TOC to 18 µg/g TOC on average), while TOC values remain similar (Table 2; Fig. 5).

The distribution of *n*-alkanes is highly variable along the section, with patterns generally not being related to lithology or depth (Fig. 5). The distribution of *n*-alkanes in lignite beds from the bottom part (LB1 and LB2) is similar, with a bimodal distribution: a

337 strong maximum at C_{35} and a sub-maximum at C_{29}. In LB3, distribution is also bimodal with
338 a maximum at C_{21} or C_{23} and strong sub-maximum at C_{35}. The lignites from the middle part
339 of the section in LB4 and LB5 have a unimodal distribution maximizing at C_{21} or C_{23}. In
340 LB6, three different patterns are recorded: a unimodal distribution maximizing at C_{25} in TP3-
341 195, at C_{21} in TP3-203 and pattern similar to those reported in LB1 and LB2 in TP3-216.
342 Clayey samples TP1-22, TP3-157 and TP3-176 show a unimodal distribution maximizing at
343 C_{25} or C_{27}, whereas the distribution is affected by an unusual amount of C_{18} in most of the
344 others, leading to a bimodal and even trimodal distribution in TP3-224 that results from a
345 strong contribution of C_{35} (Fig. 5). In particular, the two trunk/root samples (TP1-65 and
346 TP1-114) show similar patterns clearly maximizing at C_{23}.

347 Most of the samples have a marked odd/even predominance in the range C_{21} to C_{35}.
348 They often exhibit Carbon Preference Indices (CPI) higher than 2 and sometimes reaching
349 5.5 (Table 2). This odd predominance is mainly driven by the longest homologues ($> C_{25}$),
350 which are usually attributed to higher plant leaf-wax input (Eglinton et al., 1962; Eglinton
351 and Hamilton, 1967; Meyers, 1997). Shorter-chain *n*-alkanes ($<C_{21}$) – generally attributed to
352 algal/bacterial sources (Blumer et al., 1971; Cranwell et al., 1987; Giger et al., 1980; Meyers,
353 1997; Ladygina et al., 2006) – are in relatively low amounts (24 wt. % $\pm$ 15%) when
354 compared to *n*-alkanes above C_{21}.

355 The ACL values of the *n*-alkanes were calculated over the range C_{21}-C_{35} to cover the
356 range of *n*-alkanes found in aquatic and terrestrial plants (e.g., Eglinton and Hamilton, 1967;
357 Ficken et al., 2000; Diefendorf et al., 2011). ACL values range between 22.4 and 31.8 (Table
358 2; Fig. 5). A similar trend is observed for the evolution of the ACL values and that of the
359 amount of *n*-alkanes, *i.e.* the ACL and *n*-alkane amounts show maximal values in LB1 to
360 decrease toward LB4 and LB5. Another minimal value is observed for LB6, before it
361 increases again to the top of the section.

Pristane (Pr) and phytane (Ph) were detected in all samples in small amounts at level of ~9 and ~8 µg/g TOC on average, respectively (not shown). Pr/Ph ratios show large variations, ranging from 0.3 in clayey samples with poor organic matter content up to 7.6 in a lignite. The highest values are observed in lignites or clayey OM-rich samples (Table 2).

3.5. Compound-specific hydrogen isotopes (δ^2H)

δ^2H values were determined for C_{17} to C_{35} *n*-alkanes and for the isoprenoid pristane and phytane (Table 3; Fig. 6). Results for *n*-alkanes as well as pristane and phytane are reported along the section in Fig. 7.

3.5.1. Alkanes

δ^2H values range between −248 and −151 ‰. Maximal variability is observed for *n*-C_{27} with 90 ‰ between minimum (−242 ‰) and maximum (−152 ‰) values. The variability of δ^2H values is also high for *n*-C_{19} to *n*-C_{25} (Fig. 6). In addition, the longer the chain, the more ^{2}H-enriched are the *n*-alkanes, except for the *n*-C_{35}. The latter is ^{2}H-depleted when compared to common vascular plant *n*-alkanes (C_{27} to C_{31}, Eglinton and Hamilton, 1967), but is still ^{2}H-enriched when compared to $<C_{27}$ *n*-alkanes.

Along the section, δ^2H values exhibit generally parallel trends (Fig. 7). In detail, three main features are recorded. First, the offset between δ^2H values of two groups of *n*-alkanes increases from the base of LB1 to the base of LB5: the most negative values are recorded for *n*-alkanes $<C_{25}$, whereas longer chain *n*-alkanes show more positive values. Second, δ^2H values of all the *n*-alkanes increase drastically in the intercalated organic-rich clayey layer in LB5 (TP3-157) and then remain at almost constant high values (−174 ±11 ‰) until LB6. At this point, δ^2H decreases to lower values (−191 ±17 ‰) before increasing again in the overlaying clayey layer (−169 ±10 ‰). This general increase in δ^2H values occurs for all the

386 *n*-alkanes. Third, lower δ^2H values were measured in lignites, alternating with higher values
387 measured in clayey layers and trunk/root samples (Fig. 6). However, this feature is less
388 obvious for *n*-alkanes >C_{27}.
389
390 *3.5.2. Isoprenoids*
391 The δ^2H values of pristane and phytane range between −303 and −260 ‰ (−283 ‰ on
392 average) and between −311 and −233 ‰ (−274 ‰ on average), respectively. Pristane and
393 phytane are systematically ^{2}H-depleted when compared to *n*-alkanes with Δ^2H = −80 ‰ on
394 average, where Δ^2H is the difference between the average δ^2H value of the isoprenoids and
395 the average δ^2H value of the *n*-alkanes (Fig. 6).

396 *3.6. brGDGT*

397 The brGDGTs required for MAAT calculation were detected and could be quantified
398 in only 7 samples (see supplementary data for details). They represent the oldest GDGTs ever
399 recorded to date (Schouten et al., 2013). The use of this proxy is therefore attempted for the
400 first time in the Early Jurassic and must be taken with caution. According to the calibration of
401 Weijers et al. (2007), MAATs range between -1.1 °C and 18.0 °C, while they range between
402 4.0 °C and 15.9 °C based on the Peterse et al. (2012) calibration (Table 2). Although they
403 show the same trends, negative MAATs values during the Early Jurassic are very unlikely.
404 Thus, the first set of MAATs values will not be further considered, and only trends will be
405 considered for the second one. Here, an increasing trend was observed during the early
406 Toarcian (cf. Fig. 9).

4. Discussion

4.1. Preservation of organic matter

The organic matter is mainly immature (T_{max} <440 °C) and experienced a limited burial, allowing paleoenvironmental interpretations (Espitalié et al., 1985, see supplementary data 1). Higher HI values in lignites as compared to clayey layers suggest a relatively better organic matter preservation in lignites, although a matrix mineral effect in clayey layers leading to lower HI values cannot be excluded (Espitalié et al., 1985). However, higher OI values in clayey layers relative to lignites are in agreement with a slightly less preserved organic matter in clayey layers, probably resulting from oxidative conditions at the water-sediment interface or during transport processes for silty-sediments (Espitalié et al., 1985). In addition, no significant correlation was recorded between $\delta^{15}N$ values and either TOC or TN values (n=52; p>>0.05), suggesting a relative independence between the isotopic composition and the organic content.

The $\delta^{2}H$ values of individual lipid biomarkers are much less prone to diagenetic alteration when compared to bulk organic matter, because (i) specific compounds are not influenced by preferential degradation of less stable compounds (Andersen et al., 2001) and (ii) hydrogen in lipids is strongly bound to carbon and considered non exchangeable, which allows the conservation of the primary $\delta^{2}H$ values of lipids at temperatures above 150 °C (Schimmelmann et al., 1999). To this respect, Dawson et al. (2004) reported *n*-alkanes and isoprenoids that retained their original $\delta^{2}H$ values in relatively immature torbanites as old as the Late Carboniferous.

It has been suggested that the transfer of hydrogen from water to organic matter is the most important mechanism leading to hydrogen-isotope exchange (Schimmelmann et al., 2006), whereas hydrogen is thought to be totally exchanged on very long geological timescale (hundreds of million years, Koepp, 1978; Sessions, 2016). This mechanism leads to

the homogenization of δ^2H values of specific compounds, thus overprinting their primary δ^2H values (Yang and Huang, 2003; Sessions et al., 2004; Pedentchouk et al., 2006). In Taskomirsay, such a homogenization of δ^2H values was not observed as indicated by both the large variability in δ^2H values of homologous *n*-alkanes (up to 90 ‰) and between adjacent sedimentary layers (i.e. samples TP2-140 *vs.* TP3-151; Fig. 6 and 7). The high CPI (>1) also argues against post-depositional alteration of the δ^2H values (Pedentchouk et al., 2006). Most importantly, an offset (Δ^2H = 80 ‰ on average, Fig. 6) between the δ^2H values of *n*-alkanes and isoprenoids was recorded. In Taskomirsay, this offset is similar to the offset recorded in modern biological samples (Sessions et al., 1999; Chikaraishi et al., 2004) and rules out any extensive homogenization of δ^2H values (Andersen et al., 2001; Dawson et al., 2004; Sessions et al., 2004).

On the basis of these lines of evidence, we can conclude that the organic proxies mainly reflect primary environmental signals, thus allowing paleoenvironmental interpretations.

4.2. Sources of organic matter

The sporomorph associations as well as fossil woods argue for a well-developed terrestrial macro-paleoflora. The presence of *Xenoxylon* from LB2 to the transition zone, inferred from fossil woods, is also confirmed by infra-millimeter wood fragments, belonging to *Xenoxylon*, observed in palynological slides (Schnyder et al., accepted). After the transition zone, lacustrine areas are suggested by sedimentology and the presence of *Botryococcus* sp. and *Ovoidites* from ~45 m (Schnyder et al., accepted). However, the Type-III organic matter points to a major contribution of vascular plants to the organic matter through the entire section (Fig. 3; Espitalié et al., 1985), confirmed by (i) woods *in situ*, (ii) wood fragments

455 associated with sporomorphs (Schnyder et al., accepted) and (iii) the combination of atomic
456 C/N ratios and $\delta^{13}C_{org}$ values (Tyson, 1995; Meyers, 1997; Fig. 8).

457 The terrestrial origin of the organic matter is confirmed at the molecular level by the
458 distribution of *n*-alkanes dominated by $>C_{21}$ *n*-alkanes associated with CPI >1 (Eglinton and
459 Hamilton, 1967; Ficken et al., 2000; Diefendorf et al., 2011), whereas a minor algal/bacterial
460 contribution is deduced from the relatively low amount of shorter chain *n*-alkanes, except in
461 clayey and OM poor samples where *n*-C_{18} usually dominates (Fig. 5; Blumer et al., 1971;
462 Cranwell et al., 1987; Giger et al., 1980; Meyers, 1997; Ladygina et al., 2006). Despite
463 various possible sources of pristane and phytane, Pr/Ph ratios <1 observed in those samples
464 are consistent with the development of bacteria in anoxic/suboxic hypersaline environments,
465 whereas Pr/Ph ratios >>1 in OM-rich sediments agree with a terrestrial organic matter
466 deposited in oxic environments (Table 2; Didyk et al., 1978; Peters et al., 2005; Riboulleau et
467 al., 2007).

468 Long-chain *n*-alkanes (C_{27}, C_{29}, C_{31}) are usually attributed to land-plant waxes (Eglinton
469 et al., 1962; Eglinton and Hamilton, 1967). In Taskomirsay, they are likely produced by
470 gymnosperms since the major diversification of angiosperms occurred much later, during the
471 Early Cretaceous (Gee, 2000), about 50 My after the study period. However, long-chain *n*-
472 alkanes (C_{27}-C_{31}) with strong odd/even carbon predominance could also result from an algal
473 input (e.g., *Botryococcus* spp., Lichtfouse et al., 1994; Riboulleau et al., 2007). Thus, an algal
474 influence on the long-chain *n*-alkanes in TP3-224 cannot be ruled out, in agreement with the
475 lowest C/N ratio recorded (C/N = 38) in the section.

476 *n*-Alkanes C_{21} to C_{25} are generally predominant in lignites and trunk/root samples from
477 LB3 to the base of LB6 (Fig. 5). They have been reported to originate from modern
478 *Sphagnum* (Baas et al., 2000; Nott et al., 2000) and aquatic macrophytes (Ficken et al., 2000;
479 Bechtel et al., 2007), thus representing an aquatic environment. But, sphagnums are unlikely

important sources for those *n*-alkanes, because they radiated during the Miocene and only rare fossils and spores related to proto-sphagnums have been reported in the Mesozoic (Shaw et al., 2010). Alternatively, mosses might be a valuable source of these *n*-alkanes since they have been recognized at least from the lower Carboniferous (Thomas, 1972). However, no sporomorph of mosses or sphagnums could be recognized (Schnyder et al., accepted).

The major contribution of the C_{23} in most of the samples (Fig. 5) is more likely attributed to conifers as this distribution is close to the general trend observed in the latter, with maxima at C_{23} and C_{25} (Oros et al., 1999; Nakamura et al., 2010). This is supported by the unimodal distribution maximizing at C_{23} observed in the two trunk/root samples TP1-65 and TP1-114. Further evidence come from the high concentration of fossil trunks/roots in life positions through the section in agreement with peaty/swampy forests – inferred from the numerous coal-rich formations in the North Hemisphere – characterizing the Early Jurassic (Miao et al., 1989; Rees et al., 2000; Wang et al., 2005). In addition, C_{20}-C_{23} alkanes have been reported in Carboniferous coalified paleoflora (Disnar and Harouna, 1994), in Carboniferous-Permian terrigenous/coaly sediments (Scheffler et al., 2003), and in the Late Oligocene *Taxodium dubium* (*Cupressaceae s.l*) fossil plant maximizing at C_{21} (Stefanova et al., 2013). The first authors attributed the Carboniferous coals to Paleozoic Gondwana swamp flora made of conifer precursors, whereas Stefanova et al. (2013) emphasized that *Taxodium dubium* was known in marshy environments and flooded lowland terrains. Finally, the distribution of *n*-alkanes in *Xenoxylon* fossil woods collected in the Bajocian/Callovian of Poland and Germany – paleoecologically related to environments with no water restriction, usually riparian forests and swamps (Oh et al., 2015) – also maximizes at C_{23} (Marynowski et al., 2008), although these authors attributed the presence of *n*-alkanes to contaminations by host clays. This is not the case here when compared the root/trunk TP1-65 to its host clays (TP1-65bis) as they show large differences in their *n*-alkane distribution (Fig. 5). To our opinion,

all these lines of evidence support the hypothesis that C_{21}–C_{23} *n*-alkanes in our samples could result from conifers like *Xenoxylon* that thrived in flooded environments.

In summary, those evidences support the use of *n*-C_{21}–*n*-C_{23} as representing an environment under an almost permanent shallow water layer, and the use of *n*-C_{27}–*n*-C_{31} as strictly terrestrial vascular plant biomarkers (eg. Ficken et al., 2000; Sachse et al., 2004; Mügler et al., 2008). Accordingly, C_{21}–C_{23} *n*-alkanes will be considered as deriving from an "aquatic pool" and C_{27}–C_{31} *n*-alkanes from a "terrestrial pool", respectively, for this study. As δ^2H values of C_{23} and C_{27} *n*-alkanes were accurately measured for all samples, they will be considered as representative of the aquatic and terrestrial pool, respectively.

The existence of these two different pools could explain the offset between the δ^2H values of the ^{2}H-depleted aquatic pool and the ^{2}H-enriched terrestrial pool (Fig. 6 and 7). ^{2}H-enriched C_{27}–C_{31} *n*-alkanes suggest hydrogen loss by evaporation and/or vascular plant transpiration (Sachse et al., 2004, 2006), whereas the ^{2}H-depleted C_{21}–C_{23} *n*-alkanes suggest that they originate from organisms that do not evapotranspire (e.g., aquatic macrophytes; Ficken et al., 2000; Nott et al., 2000; Bechtel et al., 2007) or from organisms living in high relative humidity sub-environments (e.g., ombrotrophic peatlands; Nichols et al., 2009).

The origin of the C_{33} and C_{35} *n*-alkanes that are dominant at the base and at the top of the section (Fig. 5) is uncertain as such a predominance has never been reported in sediments to date. However, these homologues were found to be major *n*-alkanes in some modern *Cupressaceae* (Dodd et al., 1998; Diefendorf et al., 2011; Street et al., 2013), suggesting a terrestrial higher plant origin for these compounds. The relatively high δ^2H signal of those compounds is in agreement with a vascular plant origin that would be subject to evapotranspiration.

529 *4.3. Paleoclimate evolution*

530 The Taskomirsay section is separated into three parts for discussion purposes. The
531 first part includes the base of the section to the base of the transition zone at ~26 m and is
532 named "Phase 1". It corresponds to the mid- to late Pliensbachian (Fig. 9; Schnyder et al.,
533 accepted). The second part is the transition zone, corresponding to the transition between
534 Pliensbachian and Toarcian, based on sporomorph associations and $\delta^{13}C_{org}$ (Fig. 9; Schnyder
535 et al., accepted). The $\delta^{13}C_{org}$ curve is described in Schnyder et al., accepted. The transition
536 zone ends at ~35 m. The rest of the section, corresponding to the early Toarcian is named
537 "Phase 2" (Fig. 9).

538

539 *4.3.1. Paleoflora*

540 The morphogenus conifer *Xenoxylon* Gothan is biogeographically related to cool/humid
541 settings and thus, usually to high latitudes (Philippe and Thévenard, 1996; Philippe and
542 Tchoumatchenco, 2008; Philippe et al., 2009). Recent isotopic studies confirmed these
543 paleoclimatic requirements for *Xenoxylon* (Amiot et al., 2015). In addition, *Xenoxylon*
544 occurred at lower latitudes during the Jurassic and even thrived in Western Europe during
545 cold episodes, such as in the late Pliensbachian or in the early Oxfordian (Philippe and
546 Thévenard, 1996). Therefore, the occurrence of *Xenoxylon* at mid-latitudes in Taskomirsay in
547 Phase 1 and in the transition zone suggests a cool/humid period, followed by less humid
548 and/or warmer conditions in the early Toarcian (Phase 2), deduced from the demise of
549 *Xenoxylon* (Fig. 9).

550 During the Jurassic, the Euro-Sinian (West-Kazakhstan) and the West-Siberian (East-
551 Kazakhstan) floral provinces were separated by a NW/SE axis through Kazakhstan
552 (Vakhrameev, 1991) that may have fluctuated in the Jurassic (Kirichkova and Doludenko,
553 1996). Sporomorph associations (Schnyder et al., accepted) prior to the transition zone

554 suggest an influence of the West-Siberian province with a monotonous flora dominated by
555 ferns, few Cycadales, Ginkgoales, Czekanowskiales, Bennettitales and Coniferales,
556 characteristic of a moderate-warm climate (Vakhrameev, 1991), in agreement with the
557 occurrence of *Xenoxylon* in the same part of the section (Fig. 9). The influence of the Euro-
558 Sinian province (warm-temperate) progressively increased through the section with the
559 emergence of *Manumia delcourtii* (Pocock) (Dybkjaer, 1991) and later of *Ischyosporites*
560 *variegatus* (Couper) (Schulz, 1967) in Phase 2, which is one of the taxon used to identify the
561 early Toarcian (Schnyder et al., accepted). Then, the early Toarcian (Phase 2) is marked by
562 the occurrence of more thermophilic taxa such as *Callialasporites* spp. or *Ischyosporites*
563 *variegatus*, while a slight decrease in humidity is recorded by rare *Corollina* spp., associated
564 with the demise of *Xenoxylon* (Fig. 9; Schnyder et al., accepted). Accordingly, a similar
565 climatic trend has been evidenced regionally by other palynological studies during the Early
566 Jurassic in Central Asia (Iljina, 1985; Vakhrameev, 1991; Mogutcheva, 2014). Thus, globally
567 humid conditions along the section probably favored high production of biomass that enabled
568 the formation of the numerous lignite beds (Flores, 2002; Kalaitzidis et al., 2004).
569 Alternatively, changes in depositional environments or taphonomic conditions could have
570 driven the occurrence of the wood *Xenoxylon* and the mentioned sporomorphs. But, there is
571 no evidences to such hypothesis as no drastic changes in depositional environments occurred
572 until the top of the section, where lacustrine conditions took place. Most importantly, the
573 other organic markers do support a climatic interpretation of the data (see below) together
574 with other regional paleobiogeographical studies mentioned above.
575
576 *4.3.2. What do $\delta^{15}N$ values record?*
577 Many studies have concluded that the $\delta^{15}N_{org}$ values in terrestrial environments are
578 mainly driven by climate via water-availability and nutrient cycling, the $\delta^{15}N$ of plants and

soils being correlated negatively with precipitation and positively with temperatures (Austin and Vitousek, 1998; Handley et al., 1999; Amundson et al., 2003; Swap et al., 2004; Liu and Wang, 2008). In brief, $\delta^{15}N_{org}$ values in humid environments are driven by intense N-recycling between dead and alive biomass through a rapid turnover of a small N-mineral pool, whereas this cycle is interrupted in arid environments (low biomass activity) leading to N-excess in a large mineral pool (Austin and Vitousek, 1998; Handley et al., 1999; Swap et al., 2004). The latter is then subjected to N-loss by leaching and gas emission leading to high $\delta^{15}N$ values in the remaining N-pool (Handley et al., 1999; Aranibar et al., 2004). In turn, $\delta^{15}N_{org}$ values are controlled by the relative openness of the N-cycle by changes in water- or N-availability as illustrated by Martinelli et al., 1999, who reported significant higher $\delta^{15}N_{org}$ (+6.5 ‰) values in humid tropical forests (N-excess) than in temperate forests (N-limited). Considerable variations exist in $\delta^{15}N$ values from one site to another, ranging from around −8 to +22 ‰ in actual soil organic matter (Craine et al. 2015).

In Taskomirsay, $\delta^{15}N_{org}$ values were calculated for samples in which TOC is <20 % and do not strongly differ from the $\delta^{15}N_{tot}$ values, justifying the use of $\delta^{15}N_{tot}$ values as representative of the $\delta^{15}N_{org}$ values (Fig. 2), except for TP3-224 that might be influenced by an algal contribution and hence will not be considered for paleoclimate reconstructions. In the light of the previous interpretations, the relatively low and stable $\delta^{15}N_{org}$ values (~+3 ‰) – when compared to those compiled by Handley et al. (1999) in arid to semi-arid sites (>+5 ‰) – are in agreement with a globally closed N-cycle, suggesting humid conditions and/or limited nutrients in the system.

Although $\delta^{15}N_{org}$ values remain in a rather narrow range (~2.5 to ~3.5 ‰), the small excursions recorded in $\delta^{15}N_{org}$ values, either negative (LB1, LB2 and LB6) or positive (LB5), together with the scattered feature in LB4 and LB3 might reflect the tenuous equilibrium between water-availability and nutrient cycling. This pattern would imply that (i) despite

paleoflora indices in Phase 2, no drastic changes occurred along the section whether in the nutrient dynamics or regarding water-availability (Fig. 9), (ii) the vegetation has adapted to environmental changes ensuring an efficient N-recycling and thus almost constant $\delta^{15}N_{org}$ values. The latter hypothesis suggests a strong influence of the local environment on $\delta^{15}N_{org}$ values as suspected by Amundson et al. (2003), who compiled $\delta^{15}N$ values of modern plants and soils. The influence of local environments is supported by the high variability of $\delta^{13}C_{org}$ values, especially in LB4 and fossil woods (Fig. 9), which could result from changes of vegetation assemblages or changes of ^{13}C-fractionation rate tuned by temperature, altitude and/or relative humidity (Warren et al., 2001; Bowen and Revenaugh, 2003; Bowling et al., 2008). A better sampling resolution for biomarkers studies would help to decipher the real causes of variability of the $\delta^{13}C_{org}$ values, while a global and long-term influence is suggested by Schnyder et al. (accepted) to highlight the recognition of the Pliensbachian-Toarcian transition.

To sum up, no drastic changes in the $\delta^{15}N_{org}$ are recorded as compared to those reported in the Paleocene-Eocene (Storme et al., 2012) or in the Eocene-Oligocene (Tramoy et al., 2016) that exhibit much higher variations in amplitude of up to 6 ‰.

4.3.3. Molecular response of plants

Leaf waxes are produced by plants as a protection against external environment, especially to prevent water loss. Accordingly, lower production of *n*-alkanes along with shorter chain lengths is believed to reflect a decreasing need for protection against water loss and/or a deficiency of energy for biosynthesizing long chain *n*-alkanes (Weete et al., 1978; Gagosian and Peltzer, 1986; Gauvrit and Gaillardon, 1991; Shepherd and Wynne Griffiths, 2006), indicative of humid conditions. Conversely, higher amounts of *n*-alkanes and higher ACL values suggest water stress for plants, drier conditions and higher temperatures. In this

629 respect, decreasing ACL values and *n*-alkane amounts from Phase 1 to the transition zone
630 suggest increasing humidity and decreasing temperatures (Fig. 9). Then, increasing ACL
631 values and *n*-alkane amounts point to drier conditions and higher temperatures in the early
632 Toarcian (Phase 2). MAATs, reconstructed based on brGDGTs distributions, depict the same
633 trends with decreasing temperatures in Phase 1 and increasing temperatures in Phase 2,
634 although the number of samples is limited. It is noteworthy that relations between ACL
635 values and *n*-alkane amounts are particularly robust in lignites, whereas no correlation exists
636 for clayey layers (Fig. 10). In order to explain this discrepancy, we hypothesize that the
637 organic matter in swampy forest is dominated by autochthonous vascular plant inputs,
638 responding promptly to relative changes in humidity, whereas organic matter in clayey layers
639 could contain significant part of allochthonous plant products or algal/bacterial organic
640 matter (*n*-C_{18}; Fig. 5) that is less influenced by water loss (Hoffmann et al., 2013). Notice that
641 the highest amount of *n*-alkanes was recorded in the clayey layer TP1-65, which is very poor
642 in organic matter (<0.05 %). As the amount of *n*-alkanes is expressed relative to %TOC, the
643 very low %TOC results in a very high concentration of *n*-alkanes in this specific sample.
644
645 *4.3.4. Interpretation of n-alkane δ^2H values*
646 According to Sachse et al. (2012), the δ^2H values of higher plant *n*-alkanes are mainly
647 influenced by (i) the δ^2H values of precipitation (Huang et al., 2004; Sachse et al., 2004,
648 2012), (ii) the extent of evapotranspiration from soils and leaves (Smith and Freeman, 2006;
649 Feakins and Sessions, 2010) and (iii) to a minor extent, by the interspecies variability (Smith
650 and Freeman, 2006; Chikaraishi and Naraoka, 2007). δ^2H values of precipitations are
651 positively correlated with temperature at the precipitation site and negatively correlated with
652 the amount of precipitation and with the distance from the shore line (Dansgaard, 1964;
653 Epstein and Yapp, 1976; Gat, 1996; Sachse et al., 2004). Also, the amount of precipitation is

654 the most important factor in low latitudes, whereas the temperature effect predominates in
655 higher latitudes (Sachse et al., 2012). At the global scale, a latitudinal/climatic distribution
656 pattern of δ^2H values has been reported in modern precipitation patterns and also for
657 geological times with δ^2H values being negatively correlated with latitudes (Bowen and
658 Revenaugh, 2003; Dawson et al., 2004).

659 The terrestrial signal in our samples is expressed by the absolute δ^2H values of the *n*-
660 alkane C_{27} (−242 to −151 ‰; −192 ± 21 ‰), which are closer to those reported from the
661 Paleocene-Eocene at mid-latitudes in the intracontinental Bighorn Basin (−195 to −185 ‰;
662 Smith et al., 2007) and at high latitudes in the Arctic (−210 to −160 ‰, Pagani et al., 2006),
663 than those reported for the same period in coastal regions from mid- to low-latitudes (–165 to
664 −140 ‰; Handley et al., 2012; −174 to −112 ‰; Garel et al., 2013). They are also closer to
665 early Permian δ^2H values recorded in high latitudes with glacial to cool-temperate
666 environments (*ca*. −200 ‰), than those recorded for the same period in tropical regions (Fig.
667 6*; ca*. −150 ‰; Dawson et al., 2004; *ca*. −100 ‰; Izart et al., 2012). These results are in
668 agreement with the estimated mid-paleolatitudes of the Taskomirsay section (36° N ± 8°,
669 Bruno Vrielynck, pers. comm., 2014), associated with a warm to cool-temperate global
670 climate during the Early Jurassic at those paleolatitudes (Rees et al., 2000). It may also point
671 to the intra-continental character of the Karatau Basin during the Pliensbachian-Toarcian.

672 Considering these paleolatitudinal/paleoclimatic settings, the location of the Karatau
673 Basin during the Jurassic (~40° N) and the large excursions of the δ^2H values, air
674 temperatures and precipitation amount were probably both important factors driving
675 precipitation δ^2H values. Then, δ^2H values of *n*-alkanes were more or less affected by
676 evapotranspiration with respect to their environment whether aquatic or terrestrial (Sachse et
677 al., 2006; Smith and Freeman, 2006; Feakins and Sessions, 2010). To constrain the

678 evapotranspiration effect of terrestrial plants, the aquatic *n*-C_{23} will be considered for
679 paleohydrological reconstructions.

680 δ^2H values of *n*-alkanes are usually well correlated with that of the source water used by
681 organisms and thus constitute good markers for paleohydrological reconstructions (Sachse et
682 al., 2004; Mügler et al., 2008; Aichner et al., 2010; Nichols et al., 2010; Sachse et al., 2012).
683 Because the *n*-C_{23} is associated with the aquatic pool in the study section, its low δ^2H values
684 (−248 to −168 ‰; −201 ± 25 ‰, similar to *n*-C_{21} δ^2H values) argue for very humid
685 conditions either in a cool-temperate or glacial climate regime (Fig. 6). However, no
686 sedimentological evidence has been found for a glacial environment, and this kind of
687 environment is highly inconsistent with plant assemblages in Taskomirsay (Schnyder et al.,
688 accepted). Thus, cool-temperate conditions are most likely, whereas the very negative δ^2H
689 values could reflect a long distance from the source water (Gat, 1996). Although the exact
690 distance from the shore line is currently unknown (either to the South or West), it is most
691 probably on the order of tens to hundreds of kilometers (B. Vrielynck, pers. Comm., 2014).

692 Along the section, the decrease in *n*-C_{23} δ^2H values from the base of the section to the
693 transition zone could result from a decrease in source-water δ^2H values, indicating an
694 increase in humidity and decrease in temperature, the coolest/most humid interval being
695 recorded from LB4 to the base of LB5 within the transition zone (−236 ± 11 ‰; Fig. 9).
696 Then, a strong increase in *n*-C_{23} δ^2H values (−188 ± 18 ‰) suggests relatively drier
697 conditions in the early Toarcian, associated with higher temperatures. ACL values are in
698 agreement with those two general trends. Nevertheless, slightly lower *n*-C_{23} δ^2H values in
699 LB6 (−209 ± 6 ‰) suggest a more humid period that favored swampy environments. But,
700 those δ^2H values are ~27 ‰ higher than in LB4/LB5, probably resulting from the deposition
701 of LB6 in warmer conditions instead of drier conditions. This interpretation is supported by

concomitant thermophilic paleoflora and increasing temperatures recorded by GDGTs in the early Toarcian (Fig. 9).

At high frequency, higher δ^2H values intercalated in clayey layers may represent local changes in sub-environments between lignites and clayey layers with more humid conditions for lignites than for clays (Fig. 7 and 9). Whereas paleoclimatic variations may have overprinted local changes at a broader scale when taking into account differences in δ^2H values between the different sedimentary cycles.

4.3.5. Paleoclimate reconstructions based on $\Delta^2H_{ter\text{-}aq}$

The influence of relative humidity and temperature on δ^2H values is also recorded by the evapotranspiration of the ecosystem (Sachse et al., 2006; Mügler et al., 2008). The ecosystem evapotranspiration can be evaluated by the hydrogen isotopic difference between terrestrial *n*-alkanes and aquatic *n*-alkanes, based on two assumptions: (i) in a given ecosystem, water source is the same for terrestrial and aquatic organisms and (ii) aquatic and terrestrial organisms synthesize their *n*-alkanes with the same biosynthetic fractionation ($\varepsilon = -157$ ‰; Sachse et al., 2006). However, terrestrial flora synthetize their *n*-alkanes from ^{2}H-enriched leaf-water after soil evaporation and leaf-transpiration, leading to ^{2}H-enrichment of long-chain *n*-alkanes (eg. Sachse et al., 2006). Indeed, *n*-alkanes from surface sediments of European lakes showed an isotopic difference as large as +30 ‰ between the terrestrial and the aquatic pool (Sachse et al., 2004, 2006).

In the Taskomirsay samples, evapotranspiration was estimated from the isotopic difference between δ^2H values of the C_{27} and the C_{23} *n*-alkanes and was noted as $\Delta^2H_{ter\text{-}aq}$ (Fig. 9). Notice that the aquatic pool defined for this study differs from that of the other studies by the origin of the aquatic *n*-alkanes, which are attributed here to swampy or riparian

vegetation with no water restriction (*e.g.*, *Xenoxylon* vegetation type; Oh et al., 2015). Contributions from mosses and aquatic plants are also possible. The $\Delta^2H_{ter\text{-}aq}$ was always positive in lignites, up to +76 ‰ in LB4, whereas it remained close to 0 ‰ or slightly negative in clayey layers. According to Mügler et al. (2008), who calculated $\Delta^2H_{ter\text{-}aq}$ values in a Tibetan lake, positive $\Delta^2H_{ter\text{-}aq}$ values are typical for humid environments. They result from evapotranspiration of terrestrial vegetation leading to ^{2}H-enrichment in the terrestrial pool, whereas ^{2}H-enrichment of the aquatic pool is limited by low evaporation rates. $\Delta^2H_{ter\text{-}aq}$ values in the section are thus in agreement with humid conditions. In contrast, under arid to semi-arid conditions, significant ^{2}H-enrichment occurs in the aquatic pool relatively to the terrestrial pool, resulting from long term lake water evaporation, which counterbalances plant evapotranspiration: a negative $\Delta^2H_{ter\text{-}aq}$ is thus recorded (~−60 ‰; Mügler et al., 2008; Rao et al., 2014). Because the most negative $\Delta^2H_{ter\text{-}aq}$ recorded did not exceed −6 ‰, arid to semi-arid conditions during deposition of clayey layers are unlikely and generally humid conditions are suggested, in agreement with paleoflora, $\delta^{15}N_{org}$ and absolute δ^2H values.

In addition, maximal $\Delta^2H_{ter\text{-}aq}$ positive values (+41 and +76 ‰ in LB4), suggest a considerable evapotranspiration rate (Fig. 9). This interpretation is in apparent contradiction with the coolest/most humid interval deduced from low δ^2H values of *n*-alkanes from the aquatic pool and low $\delta^{15}N_{org}$ values. A possible explanation for this discrepancy is that higher input of allochthonous terrestrial *n*-alkanes from distant areas with a heavier isotopic composition of meteoric water might have led to higher $\Delta^2H_{ter\text{-}aq}$ (~70 ‰; Sachse et al., 2004). Alternatively, high $\Delta^2H_{ter\text{-}aq}$ could be explained by seasonal differences in water uptake and *n*-alkane production between the aquatic and terrestrial pools (Jacob et al. 2007), which is typical under temperate climate-regime. Indeed, higher plant *n*-alkanes are mostly produced during the growing season in spring and summer (Sachse et al., 2004, 2009), *i.e.* under relatively drier/warmer conditions, which could account for the production of ^{2}H-

751 enriched long-chain *n*-alkanes. Conversely, the aquatic pool of *n*-alkanes might have been
752 produced under more humid/cool conditions during a wet season, which could explain their
753 low δ^2H values (Fig. 9).

754 The hypothesis of alternating wet/dry season responsible for high $\Delta^2H_{ter\text{-}aq}$ could also
755 explain the scatter in $\delta^{15}N_{org}$ values in LB4 by the dual influences of wet and dry seasons
756 (Swap et al., 2004): (i) low N-recycling rate during dry season, leading to N mineralization
757 and ^{15}N-enrichment, and (ii) intense N-recycling by microbial biomass during the growing
758 season that re-processes the accumulated N, leading to ^{15}N-depletion. In other words, if the
759 dry season effects of ^{15}N-enrichment exceed the wet season effects of ^{15}N-depletion, $\delta^{15}N$
760 values of the remaining organic matter would increase and *vice versa*. Following the
761 interpretation of $\Delta^2H_{ter\text{-}aq}$ values as a seasonal indicator, $\Delta^2H_{ter\text{-}aq}$ values close to 0 ‰ in Phase
762 2 might suggest low seasonality (Fig. 9). Precisely, recent spectral analysis of $\delta^{13}C$ values
763 measured in carbonates, used in cyclostratigraphy, revealed that astronomical configuration
764 of the Earth would have enhanced seasonality at the Pliensbachian-Toarcian transition and
765 favored low seasonality in the early Toarcian (Martinez and Dera, 2015).
766

767 **5. Reconciling proxies**

768 Proxies used in this study yield contrasting responses to the inferred climate changes.
769 An absence of drastic changes were recorded by $\delta^{15}N_{org}$ values and paleoflora revealed
770 globally humid conditions apart from slightly less humid and warmer conditions in the early
771 Toarcian. This warming was confirmed by MAATs reconstructed from brGDGTs. In
772 contrast, molecular proxies (*n*-alkane amount, ACL, δ^2H values, $\Delta^2H_{ter\text{-}aq}$ values and
773 brGDGTs) were highly variable along the section, especially δ^2H values. These proxies argue
774 for maximal humidity and minimal temperatures in the Pliensbachian-Toarcian transition.

This period could thus correspond to the cool late Pliensbachian (Bailey et al., 2003; Morard et al., 2003; Suan et al., 2010). Molecular proxies also supported drier/warmer conditions at the base of the section (middle Pliensbachian?) and in the early Toarcian as well as humid/dry cycles between lignites (humid) and clayey layers (drier).

The absence of a correlation between $\delta^{15}N_{org}$ and $\delta^{2}H$ values, which are both influenced by water availability, might point to different spatial integration of those proxies, $\delta^{15}N_{org}$ and $\delta^{2}H$ reflecting local (Szpak, 2014) and regional (precipitation regimes, air-mass temperatures; Sachse et al., 2012) influences, respectively. Sea level variations may influence $\delta^{2}H$ values of precipitation by modifying the distance between shore lines and the study area (Gat, 1996). Consequently, low sea level may increase the distance from the shore line leading to lower $\delta^{2}H$ values of the precipitation and *vice versa*, and concomitant temperature/humidity variations could lead to over- or underestimation of paleohydrological changes (e.g., Garel et al., 2013). It is therefore likely that the low sea level and the low temperatures (higher ^{2}H-fractionation) recorded in the late Pliensbachian led to an overestimation of humidity and reversely for the early Toarcian, which is marked by global warming and sea-level rising (Hallam, 1967; Hesselbo and Jenkyns, 1998; Bailey et al., 2003; Rosales et al., 2004; Suan et al., 2010). The recognition of *Botryococcus* in the uppermost part of the section and the alternation between silts and clay suggest a lacustrine/deltaic environment (Schnyder et al., accepted). This kind of environment would have been favored by the early Toarcian global transgression (Hallam, 1967; Hesselbo and Jenkyns, 1998) that increased the regional water level base and consequently buried the older sediments. Thus, variations of sea level may reconcile the drastic paleohydrological changes recorded by the $\delta^{2}H$ values and the rather stable climatic conditions implied by the $\delta^{15}N_{org}$ values. This hypothesis is strongly supported by Korte et al. (2015) who demonstrated the influence of the ocean dynamic on the global climate in the Early and Middle Jurassic.

6. Conclusions

The Taskomirsay section is a unique continental record that encompasses the Pliensbachian-Toarcian transition and contains well-preserved Type-III organic matter. Sources of organic matter were separated into two pools: (i) a purely terrestrial and (ii) an "aquatic" pool constituted of vegetation that thrived under almost permanent water supply, with possible contributions from mosses and aquatic plants.

Our multi-proxy analysis argues for globally humid condition through the section, probably under a warm- to cool-temperate regime, as constrained by *Xenoxylon* wood. However, paleoflora and δ^2H values suggest slightly less humid and warmer conditions starting from the early Toarcian, as also usually recorded in the marine realm. This interval was preceded by the probably coolest/most humid period that may correspond to the late Pliensbachian. In addition, enhanced seasonality has been hypothesized, starting from the mid-late Pliensbachian and maximizing at the Pliensbachian-Toarcian transition, in agreement with a temperate climate regime. The combination of sedimentological and organic analyses provide the most probable picture of landscapes in Taskomirsay: fluvial systems cutting through swampy forests from the base of the section (mid- to late Pliensbachian) to the transition zone (Pliensbachian-Toarcian transition) followed by relatively open lacustrine conditions in the upper part (early Toarcian).

Finally, this study sheds new light on the use of compound-specific δ^2H values in ancient sediments and stresses the complexity of the $\delta^{15}N_{org}$ as a paleoclimatic proxy. Those proxies still need to be combined with other parameters like clay mineralogy, palynofacies or other biomarker molecules (e.g., terpenoids). Paleoclimate changes should also be constrained at the regional scale with other continental sections in Central Asia to link paleoclimate changes

recorded in the marine realm to those in continental settings, even though inter-linkages could be challenging.

Acknowledgments

We thank the geological department of Namur and their members for their technical assistance with treatments for nitrogen isotopes analyses and especially Gaëtan Rochez. We are also grateful to Véronique Vaury (IEES-UPMC) for nitrogen isotopes analyses, Christelle Anquetil for GC-MS analyzes, Nicolas Brossart for IRMS, Paula Iacumin and Jean Yves Storme for preliminary nitrogen analyzes. We also thank Alexandre Lethiers for help in drawing, and Arndt Schimmelmann and the anonymous reviewer for their constructive reviews. This study was supported by EMERGENCE project from UPMC, DARIUS program and by Agence Nationale de la Recherche PalHydroMil project (ANR JCJC, 2011-2013).

References

Aichner, B., Herzschuh, U., Wilkes, H., Vieth, A., Böhner, J., 2010. δD values of *n*-alkanes in Tibetan lake sediments and aquatic macrophytes – A surface sediment study and application to a 16 ka record from Lake Koucha. Org. Geochem. 41, 779–790. doi:10.1016/j.orggeochem.2010.05.010

Al-Suwaidi, A.H., Angelozzi, G.N., Baudin, F., Damborenea, S.E., Hesselbo, S.P., Jenkyns, H.C., Manceñido, M.O., Riccardi, A.C., 2010. First record of the Early Toarcian Oceanic Anoxic Event from the Southern Hemisphere, Neuquén Basin, Argentina. J. Geol. Soc. 167, 633–636. doi:10.1144/0016-76492010-025

Amiot, R., Wang, X., Zhou, Z., Wang, X., Lécuyer, C., Buffetaut, E., Fluteau, F., Ding, Z., Kusuhashi, N., Mo, J., Philippe, M., Suteethorn, V., Wang, Y., Xu, X., 2015. Environment and ecology of East Asian dinosaurs during the Early Cretaceous inferred from stable oxygen and carbon isotopes in apatite. J. Asian Earth Sci. 98, 358–370. doi:10.1016/j.jseaes.2014.11.032

Amundson, R., Austin, A.T., Schuur, E. a. G., Yoo, K., Matzek, V., Kendall, C., Uebersax, A., Brenner, D., Baisden, W.T., 2003. Global patterns of the isotopic composition of soil and plant nitrogen. Glob. Biogeochem. Cycles 17, 1–10. doi:10.1029/2002GB001903

Andersen, N., Paul, H.A., Bernasconi, S.M., McKenzie, J.A., Behrens, A., Schaeffer, P., Albrecht, P., 2001. Large and rapid climate variability during the Messinian salinity crisis: Evidence from deuterium concentrations of individual biomarkers. Geology 29, 799–802. doi:10.1130/0091-7613(2001)029<0799:LARCVD>2.0.CO;2

858 Aranibar, J.N., Otter, L., Macko, S.A., Feral, C.J.W., Epstein, H.E., Dowty, P.R., Eckardt, F.,
859 Shugart, H.H., Swap, R.J., 2004. Nitrogen cycling in the soil–plant system along a
860 precipitation gradient in the Kalahari sands. Glob. Change Biol. 10, 359–373.
861 doi:10.1111/j.1365-2486.2003.00698.x
862 Austin, A.T., Vitousek, P.M., 1998. Nutrient dynamics on a precipitation gradient in Hawai'i.
863 Oecologia 113, 519–529. doi:10.1007/s004420050405
864 Baas, M., Pancost, R., van Geel, B., Sinninghe Damsté, J.S., 2000. A comparative study of
865 lipids in Sphagnum species. Org. Geochem. 31, 535–541. doi:10.1016/S0146-
866 6380(00)00037-1
867 Bailey, T.R., Rosenthal, Y., McArthur, J.M., van de Schootbrugge, B., Thirlwall, M.F., 2003.
868 Paleoceanographic changes of the Late Pliensbachian–Early Toarcian interval: a
869 possible link to the genesis of an Oceanic Anoxic Event. Earth Planet. Sci. Lett. 212,
870 307–320. doi:10.1016/S0012-821X(03)00278-4
871 Bassoullet, J.-P., Baudin, F., 1994. Le Toarcien inférieur: Une période de crise dans les
872 bassins et sur les plate-formes carbonatées de l'Europe du Nord-Ouest et de la Téthys.
873 Geobios, 3ème Symposium International de Stratigraphie du Jurassique 27,
874 Supplement 3, 645–654. doi:10.1016/S0016-6995(94)80227-0
875 Bechtel, A., Reischenbacher, D., Sachsenhofer, R.F., Gratzer, R., Lücke, A., 2007.
876 Paleogeography and paleoecology of the upper Miocene Zillingdorf lignite deposit
877 (Austria). Int. J. Coal Geol. 69, 119–143. doi:10.1016/j.coal.2006.03.001
878 Blumer, M., Guillard, R.R.L., Chase, T., 1971. Hydrocarbons of marine phytoplankton. Mar.
879 Biol. 8, 183–189. doi:10.1007/BF00355214
880 Bodin, S., Mattioli, E., Fröhlich, S., Marshall, J.D., Boutib, L., Lahsini, S., Redfern, J., 2010.
881 Toarcian carbon isotope shifts and nutrient changes from the Northern margin of
882 Gondwana (High Atlas, Morocco, Jurassic): Palaeoenvironmental implications.
883 Palaeogeogr. Palaeoclimatol. Palaeoecol. 297, 377–390.
884 doi:10.1016/j.palaeo.2010.08.018
885 Bowen, G.J., Revenaugh, J., 2003. Interpolating the isotopic composition of modern meteoric
886 precipitation. Water Resour. Res. 39, 1299. doi:10.1029/2003WR002086
887 Bowling, D.R., Pataki, D.E., Randerson, J.T., 2008. Carbon isotopes in terrestrial ecosystem
888 pools and CO2 fluxes. New Phytol. 178, 24–40. doi:10.1111/j.1469-
889 8137.2007.02342.x
890 Chikaraishi, Y., Naraoka, H., 2007. δ^{13}C and δD relationships among three *n*-alkyl compound
891 classes (*n*-alkanoic acid, *n*-alkane and *n*-alkanol) of terrestrial higher plants. Org.
892 Geochem. 38, 198–215. doi:10.1016/j.orggeochem.2006.10.003
893 Chikaraishi, Y., Naraoka, H., Poulson, S.R., 2004. Carbon and hydrogen isotopic
894 fractionation during lipid biosynthesis in a higher plant (Cryptomeria japonica).
895 Phytochemistry 65, 323–330. doi:10.1016/j.phytochem.2003.12.003
896 Coffinet, S., Huguet, A., Williamson, D., Fosse, C., Derenne, S., 2014. Potential of GDGTs
897 as a temperature proxy along an altitudinal transect at Mount Rungwe (Tanzania).
898 Org. Geochem. 68, 82–89. doi:10.1016/j.orggeochem.2014.01.004
899 Cranwell, P.A., Eglinton, G., Robinson, N., 1987. Lipids of aquatic organisms as potential
900 contributors to lacustrine sediments—II. Org. Geochem. 11, 513–527.
901 doi:10.1016/0146-6380(87)90007-6
902 Craine, J.M, Brookshire, E.N.J., Cramer, M.D., Hasselquist, N.J., Koba, K., Marin-Spiotta,
903 E., Wang, L., Ecological interpretations of nitrogen isotope ratios of terrestrial plants
904 and soils. Plant Soil 396, 1-26. doi:10.1007/s11104-015-2542-1
905 Dansgaard, W., 1964. Stable isotopes in precipitation. Tellus 16, 436–468.
906 doi:10.1111/j.2153-3490.1964.tb00181.x

907 Dawson, D., Grice, K., Wang, S.X., Alexander, R., Radke, J., 2004. Stable hydrogen isotopic
908 composition of hydrocarbons in torbanites (Late Carboniferous to Late Permian)
909 deposited under various climatic conditions. Org. Geochem. 35, 189–197.
910 doi:10.1016/j.orggeochem.2003.09.004
911 Didyk, B.M., Simoneit, B.R.T., Brassel, S.C., Eglinton, G., 1978. Organic geochemical
912 indicators of palaeoenviron- mental conditions of sedimentation. Nature 272, 216–
913 222.
914 Diefendorf, A.F., Freeman, K.H., Wing, S.L., Graham, H.V., 2011. Production of *n*-alkyl
915 lipids in living plants and implications for the geologic past. Geochim. Cosmochim.
916 Acta 75, 7472–7485. doi:10.1016/j.gca.2011.09.028
917 Disnar, J.R., Harouna, M., 1994. Biological origin of tetracyclic diterpanes, *n*-alkanes and
918 other biomarkers found in lower carboniferous Gondwana coals (Niger). Org.
919 Geochem. 21, 143–152. doi:10.1016/0146-6380(94)90151-1
920 Dodd, R.S., Rafii, Z.A., Power, A.B., 1998. Ecotypic adaptation in Austrocedrus chilensis in
921 cuticular hydrocarbon composition. New Phytol. 138, 699–708. doi:10.1046/j.1469-
922 8137.1998.00142.x
923 Dybkjaer, K., 1991. Palynological zonation and palynofacies investigation of the Fjerritslev
924 Formation (Lower Jurassic—basal Middle Jurassic) in the danish subbasin. DGU
925 Dan. Geol. Unders. Ser. A 4–150.
926 Eglinton, G., Gonzalez, A.G., Hamilton, R.J., Raphael, R.A., 1962. Hydrocarbon constituents
927 of the wax coatings of plant leaves: A taxonomic survey. Phytochemistry 1, 89–102.
928 doi:10.1016/S0031-9422(00)88006-1
929 Eglinton, G., Hamilton, R.J., 1967. Leaf Epicuticular Waxes. Science 156, 1322–1335.
930 doi:10.1126/science.156.3780.1322
931 Epstein, S., Yapp, C.J., 1976. Climatic implications of the D/H ratio of hydrogen in C-H
932 groups in tree cellulose. Earth Planet. Sci. Lett. 30, 252–261. doi:10.1016/0012-
933 821X(76)90252-1
934 Espitalié, J., Deroo, D., Marquis, F., 1985. La pyrolise Rock-Eval et ses applications. Revue
935 de l'Institut Français du Pétrole 563–579, 755–784.
936 Feakins, S.J., Sessions, A.L., 2010. Controls on the D/H ratios of plant leaf waxes in an arid
937 ecosystem. Geochim. Cosmochim. Acta 74, 2128–2141.
938 doi:10.1016/j.gca.2010.01.016
939 Ficken, K.J., Li, B., Swain, D.L., Eglinton, G., 2000. An *n*-alkane proxy for the sedimentary
940 input of submerged/floating freshwater aquatic macrophytes. Org. Geochem. 31, 745–
941 749. doi:10.1016/S0146-6380(00)00081-4
942 Flores, D., 2002. Organic facies and depositional palaeoenvironment of lignites from Rio
943 Maior Basin (Portugal). Int. J. Coal Geol., 31st International Geological Congress 48,
944 181–195. doi:10.1016/S0166-5162(01)00057-X
945 Gagosian, R.B., Peltzer, E.T., 1986. The importance of atmospheric input of terrestrial
946 organic material to deep sea sediments. Org. Geochem. 10, 661–669.
947 doi:10.1016/S0146-6380(86)80002-X
948 Garel, S., Schnyder, J., Jacob, J., Dupuis, C., Boussafir, M., Le Milbeau, C., Storme, J.-Y.,
949 Iakovleva, A.I., Yans, J., Baudin, F., Fléhoc, C., Quesnel, F., 2013. Paleohydrological
950 and paleoenvironmental changes recorded in terrestrial sediments of the Paleocene–
951 Eocene boundary (Normandy, France). Palaeogeogr. Palaeoclimatol. Palaeoecol. 376,
952 184–199. doi:10.1016/j.palaeo.2013.02.035
953 Gat, J.R., 1996. Oxygen and Hydrogen Isotopes in the Hydrologic Cycle. Annu. Rev. Earth
954 Planet. Sci. 24, 225–262. doi:10.1146/annurev.earth.24.1.225
955 Gauvrit, C., Gaillardon, P., 1991. Effect of low temperatures on 2,4-D behaviour in maize
956 plants. Weed Res. 31, 135–142. doi:10.1111/j.1365-3180.1991.tb01752.x

957 Gee, H., 2000. Shaking the Tree: Readings from Nature in the History of Life. University of
958 Chicago Press.
959 Giger, W., Schaffner, C., Wakeham, S.G., 1980. Aliphatic and olefinic hydrocarbons in
960 recent sediments of Greifensee, Switzerland. Geochim. Cosmochim. Acta 44, 119–
961 129. doi:10.1016/0016-7037(80)90182-9
962 Hallam, A., 1967. An Environmental Study of the Upper Domerian and Lower Toarcian in
963 Great Britain. Philos. Trans. R. Soc. B Biol. Sci. 252, 393–445.
964 doi:10.1098/rstb.1967.0028
965 Handley, L., O'Halloran, A., Pearson, P.N., Hawkins, E., Nicholas, C.J., Schouten, S.,
966 McMillan, I.K., Pancost, R.D., 2012. Changes in the hydrological cycle in tropical
967 East Africa during the Paleocene–Eocene Thermal Maximum. Palaeogeogr.
968 Palaeoclimatol. Palaeoecol. 329–330, 10–21. doi:10.1016/j.palaeo.2012.02.002
969 Handley, L.L., Austin, A.T., Stewart, G.R., Robinson, D., Scrimgeour, C.M., Raven, J.A.,
970 Heaton, T.H.E., Schmidt, S., 1999. The ^{15}N natural abundance ($\delta^{15}N$) of ecosystem
971 samples reflects measures of water availability. Funct. Plant Biol. 26, 185–199.
972 Hermoso, M., Minoletti, F., Rickaby, R.E.M., Hesselbo, S.P., Baudin, F., Jenkyns, H.C.,
973 2012. Dynamics of a stepped carbon-isotope excursion: Ultra high-resolution study of
974 Early Toarcian environmental change. Earth Planet. Sci. Lett. 319–320, 45–54.
975 doi:10.1016/j.epsl.2011.12.021
976 Hesselbo, S.P., Jenkyns, H.C., 1998. British Lower Jurassic Sequence Stratigraphy.
977 Hesselbo, S.P., Jenkyns, H.C., Duarte, L.V., Oliveira, L.C.V., 2007. Carbon-isotope record of
978 the Early Jurassic (Toarcian) Oceanic Anoxic Event from fossil wood and marine
979 carbonate (Lusitanian Basin, Portugal). Earth Planet. Sci. Lett. 253, 455–470.
980 doi:10.1016/j.epsl.2006.11.009
981 Hoffmann, B., Kahmen, A., Cernusak, L.A., Arndt, S.K., Sachse, D., 2013. Abundance and
982 distribution of leaf wax *n*-alkanes in leaves of *Acacia* and *Eucalyptus* trees along a
983 strong humidity gradient in northern Australia. Org. Geochem. 62, 62–67.
984 doi:10.1016/j.orggeochem.2013.07.003
985 Hou, J., Huang, Y., Wang, Y., Shuman, B., Oswald, W.W., Faison, E., Foster, D.R., 2006.
986 Postglacial climate reconstruction based on compound-specific D/H ratios of fatty
987 acids from Blood Pond, New England. Geochem. Geophys. Geosystems 7.
988 doi:10.1029/2005GC001076
989 Huang, Y., Shuman, B., Wang, Y., Webb, T., 2004. Hydrogen isotope ratios of individual
990 lipids in lake sediments as novel tracers of climatic and environmental change: a
991 surface sediment test. J. Paleolimnol. 31, 363–375.
992 doi:10.1023/B:JOPL.0000021855.80535.13
993 Huguet, A., Fosse, C., Laggoun-Défarge, F., Delarue, F., Derenne, S., 2013. Effects of a
994 short-term experimental microclimate warming on the abundance and distribution of
995 branched GDGTs in a French peatland. Geochim. Cosmochim. Acta 105, 294–315.
996 doi:10.1016/j.gca.2012.11.037
997 Iljina, V.I., 1985. Jurassic palynology of Siberia. Academy of Sciences of the USSR, Siberian
998 Branch. Institute of Geology and Geophysics. Publishing House "Nauka", Moscow.
999 Transactions 638, 1–237.
1000 Izart, A., Palhol, F., Gleixner, G., Elie, M., Blaise, T., Suarez-Ruiz, I., Sachsenhofer, R.F.,
1001 Privalov, V.A., Panova, E.A., 2012. Palaeoclimate reconstruction from biomarker
1002 geochemistry and stable isotopes of *n*-alkanes from Carboniferous and Early Permian
1003 humic coals and limnic sediments in western and eastern Europe. Org. Geochem. 43,
1004 125–149. doi:10.1016/j.orggeochem.2011.10.004

Jacob, J., Huang, Y., Disnar, J.-R., Sifeddine, A., Boussafir, M., Spadano Albuquerque, A.L., Turcq, B., 2007. Paleohydrological changes during the last deglaciation in Northern Brazil. Quat. Sci. Rev. 26, 1004–1015. doi:10.1016/j.quascirev.2006.12.004

Jansson, I.-M., McLoughlin, S., Vajda, V., Pole, M., 2008. An Early Jurassic flora from the Clarence-Moreton Basin, Australia. Rev. Palaeobot. Palynol. 150, 5–21. doi:10.1016/j.revpalbo.2008.01.002

Jenkyns, H.C., 1988. The early Toarcian (Jurassic) anoxic event; stratigraphic, sedimentary and geochemical evidence. Am. J. Sci. 288, 101–151. doi:10.2475/ajs.288.2.101

Kalaitzidis, S., Bouzinos, A., Papazisimou, S., Christanis, K., 2004. A short-term establishment of forest fen habitat during Pliocene lignite formation in the Ptolemais Basin, NW Macedonia, Greece. Int. J. Coal Geol. 57, 243–263. doi:10.1016/j.coal.2003.12.002

Kirichkova, A.I., Doludenko, M.P., 1996. New data on the phytostratigraphy of the Jurassic deposits of Kazakhstan. Stratigr. Geol. Korreliatsiia 4, 35–53.

Koepp, M., 1978. D/H isotope exchange reaction between petroleum and water: A contributory determinant for D/H-isotope ratios in crude oils? U.S. Geological Survey, 221–222.

Korte, C., Hesselbo, S.P., Ullmann, C.V., Dietl, G., Ruhl, M., Schweigert, G., Thibault, N., 2015. Jurassic climate mode governed by ocean gateway. Nat. Commun. 6, 10015. doi:10.1038/ncomms10015

Ladygina, N., Dedyukhina, E.G., Vainshtein, M.B., 2006. A review on microbial synthesis of hydrocarbons. Process Biochem. 41, 1001–1014. doi:10.1016/j.procbio.2005.12.007

Lichtfouse, É., Derenne, S., Mariotti, A., Largeau, C., 1994. Possible algal origin of long chain odd *n*-alkanes in immature sediments as revealed by distributions and carbon isotope ratios. Org. Geochem. 22, 1023–1027. doi:10.1016/0146-6380(94)90035-3

Liu, W., Wang, Z., 2008. Nitrogen isotopic composition of plant-soil in the Loess Plateau and its responding to environmental change. Chin. Sci. Bull. 54, 272–279. doi:10.1007/s11434-008-0442-y

Martinelli, L.A., Piccolo, M.C., Townsend, A.R., Vitousek, P.M., Cuevas, E., Mcdowell, W., Robertson, G.P., Santos, O.C., Treseder, K., 1999. Nitrogen stable isotopic composition of leaves and soil: Tropical versus temperate forests, in: Townsend, A.R. (Ed.), New Perspectives on Nitrogen Cycling in the Temperate and Tropical Americas. Springer Netherlands, pp. 45–65.

Martinez, M., Dera, G., 2015. Orbital pacing of carbon fluxes by a ~9-My eccentricity cycle during the Mesozoic. Proc. Natl. Acad. Sci. 201419946. doi:10.1073/pnas.1419946112

Marynowski, L., Philippe, M., Zaton, M., Hautevelle, Y., 2008. Systematic relationships of the Mesozoic wood genus Xenoxylon: an integrative biomolecular and palaeobotanical approach. Neues Jahrb. Für Geol. Paläontol. - Abh. 247, 177–189. doi:10.1127/0077-7749/2008/0247-0177

Marynowski, L., Smolarek, J., Bechtel, A., Philippe, M., Kurkiewicz, S., Simoneit, B.R.T., 2013. Perylene as an indicator of conifer fossil wood degradation by wood-degrading fungi. Org. Geochem. 59, 143–151. doi:10.1016/j.orggeochem.2013.04.006

Meyers, P.A., 1997. Organic geochemical proxies of paleoceanographic, paleolimnologic, and paleoclimatic processes. Org. Geochem. 27, 213–250. doi:10.1016/S0146-6380(97)00049-1

Miao, F., Qian, L., Zhang, X., 1989. Peat-forming materials and evolution of swamp sequences — case analysis of a Jurassic inland coal basin in China. Int. J. Coal Geol. 12, 733–765. doi:10.1016/0166-5162(89)90070-0

Mogutcheva, S.J., 2014. Main phytostratigraphic boundaries in the Jurassic deposits of Western Siberia. Stratigraphy and Geological correlations, 22 (3), 231–238.
Morard, A., Guex, J., Bartolini, A., Morettini, E., Wever, P. de, 2003. A new scenario for the Domerian - Toarcian transition. Bull. Soc. Geol. Fr. 174, 351–356. doi:10.2113/174.4.351
Mügler, I., Sachse, D., Werner, M., Xu, B., Wu, G., Yao, T., Gleixner, G., 2008. Effect of lake evaporation on δD values of lacustrine *n*-alkanes: A comparison of Nam Co (Tibetan Plateau) and Holzmaar (Germany). Org. Geochem. 39, 711–729. doi:10.1016/j.orggeochem.2008.02.008
Müller, P.J., 1977. CN ratios in Pacific deep-sea sediments: Effect of inorganic ammonium and organic nitrogen compounds sorbed by clays. Geochim. Cosmochim. Acta 41, 765–776. doi:10.1016/0016-7037(77)90047-3
Nakamura, H., Sawada, K., Takahashi, M., 2010. Aliphatic and aromatic terpenoid biomarkers in Cretaceous and Paleogene angiosperm fossils from Japan. Org. Geochem., Advances in Organic Geochemistry 2009 Proceedings of the 24th International Meeting on Organic Geochemistry 41, 975–980. doi:10.1016/j.orggeochem.2010.03.007
Nichols, J., Booth, R.K., Jackson, S.T., Pendall, E.G., Huang, Y., 2010. Differential hydrogen isotopic ratios of *Sphagnum* and vascular plant biomarkers in ombrotrophic peatlands as a quantitative proxy for precipitation—evaporation balance. Geochim. Cosmochim. Acta 74, 1407–1416. doi:10.1016/j.gca.2009.11.012
Nichols, J.E., Walcott, M., Bradley, R., Pilcher, J., Huang, Y., 2009. Quantitative assessment of precipitation seasonality and summer surface wetness using ombrotrophic sediments from an Arctic Norwegian peatland. Quat. Res. 72, 443–451. doi:10.1016/j.yqres.2009.07.007
Nott, C.J., Xie, S., Avsejs, L.A., Maddy, D., Chambers, F.M., Evershed, R.P., 2000. *n*-Alkane distributions in ombrotrophic mires as indicators of vegetation change related to climatic variation. Org. Geochem. 31, 231–235. doi:10.1016/S0146-6380(99)00153-9
Oh, C., Philippe, M., Kim, K., 2015. *Xenoxylon* Synecology and Palaeoclimatic Implications for the Mesozoic of Eurasia. Acta Palaeontol. Pol. 60, 245–256. doi:10.4202/app.2012.0132
Oros, D., Standley, L.J., Chen, X., Simoneit, B.R.T., 1999. Epicuticular wax compositions of predominant conifers of Western North America. Z. Naturforsch 54c, 17–24.
Pagani, M., Pedentchouk, N., Huber, M., Sluijs, A., Schouten, S., Brinkhuis, H., Sinninghe Damsté, J.S., Dickens, G.R., Expedition 302 Scientists, Backman, J., Clemens, S., Cronin, T., Eynaud, F., Gattacceca, J., Jakobsson, M., Jordan, R., Kaminski, M., King, J., Koc, N., Martinez, N.C., McInroy, D., Jr, T.C.M., O'Regan, M., Onodera, J., Pälike, H., Rea, B., Rio, D., Sakamoto, T., Smith, D.C., John, K.E.K.S., Suto, I., Suzuki, N., Takahashi, K., Watanabe, M., Yamamoto, M., 2006. Arctic hydrology during global warming at the Palaeocene/Eocene thermal maximum. Nature 442, 671–675. doi:10.1038/nature05043
Pedentchouk, N., Freeman, K.H., Harris, N.B., 2006. Different response of δD values of *n*-alkanes, isoprenoids, and kerogen during thermal maturation. Geochim. Cosmochim. Acta 70, 2063–2072. doi:10.1016/j.gca.2006.01.013
Peters, K.E., Walters, C.C., Moldowan, J.M., 2005. The Biomarker Guide: Biomarkers and isotopes in the environment and human history. Cambridge University Press.
Peterse, F., van der Meer, J., Schouten, S., Weijers, J.W.H., Fierer, N., Jackson, R.B., Kim, J.-H., Sinninghe Damsté, J.S., 2012. Revised calibration of the MBT–CBT

paleotemperature proxy based on branched tetraether membrane lipids in surface soils. Geochim. Cosmochim. Acta 96, 215–229. doi:10.1016/j.gca.2012.08.011
Philippe, M., Bamford, M., 2008. A key to morphogenera used for Mesozoic conifer-like woods. Rev. Palaeobot. Palynol. 148, 184–207.
Philippe, M., Jiang, H.-E., Kim, K., Oh, C., Gromyko, D., Harland, M., Paik, I.-S., Thévenard, F., 2009. Structure and diversity of the Mesozoic wood genus Xenoxylon in Far East Asia: implications for terrestrial palaeoclimates. Lethaia 42, 393–406. doi:10.1111/j.1502-3931.2009.00160.x
Philippe, M., Tchoumatchenco, P., 2008. Palaeoecologically significant wood genus *Xenoxylon* discovered in the East Stara Planina Mts. (East Bulgaria) Balaban Formation (Toarcian, Early Jurassic). Comptes Rendus Acad. Bulg. Sci. 61, 633–638.
Philippe, M., Thévenard, F., 1996. Distribution and palaeoecology of the Mesozoic wood genus *Xenoxylon*: palaeoclimatological implications for the Jurassic of Western Europe. Rev. Palaeobot. Palynol. 91, 353–370. doi:10.1016/0034-6667(95)00067-4
Philippe, M., Thevenard, F., Nosova, N., Kim, K., Naugolnykh, S., 2013. Systematics of a palaeoecologically significant boreal Mesozoic fossil wood genus, *Xenoxylon* Gothan. Palaeobot Palynol 193, 128–140.
Radke, J., Bechtel, A., Gaupp, R., Püttmann, W., Schwark, L., Sachse, D., Gleixner, G., 2005. Correlation between hydrogen isotope ratios of lipid biomarkers and sediment maturity. Geochim. Cosmochim. Acta 69, 5517–5530. doi:10.1016/j.gca.2005.07.014
Rao, Z., Jia, G., Qiang, M., Zhao, Y., 2014. Assessment of the difference between mid- and long chain compound specific δD *n*-alkanes values in lacustrine sediments as a paleoclimatic indicator. Org. Geochem. 76, 104–117. doi:10.1016/j.orggeochem.2014.07.015
Rees, P.., Ziegler, A.., Valdes, P.., 2000. Jurassic phytogeography and climates: new data and model comparisons. Warm Clim. Earth Hist. Camb. Univ. Press 297–318.
Riboulleau, A., Schnyder, J., Riquier, L., Lefebvre, V., Baudin, F., Deconinck, J.-F., 2007. Environmental change during the Early Cretaceous in the Purbeck-type Durlston Bay section (Dorset, Southern England): A biomarker approach. Org. Geochem. 38, 1804–1823. doi:10.1016/j.orggeochem.2007.07.006
Rosales, I., Quesada, S., Robles, S., 2004. Paleotemperature variations of Early Jurassic seawater recorded in geochemical trends of belemnites from the Basque–Cantabrian basin, northern Spain. Palaeogeogr. Palaeoclimatol. Palaeoecol. 203, 253–275. doi:10.1016/S0031-0182(03)00686-2
Sachse, D., Billault, I., Bowen, G.J., Chikaraishi, Y., Dawson, T.E., Feakins, S.J., Freeman, K.H., Magill, C.R., McInerney, F.A., van der Meer, M.T.J., Polissar, P., Robins, R.J., Sachs, J.P., Schmidt, H.-L., Sessions, A.L., White, J.W.C., West, J.B., Kahmen, A., 2012. Molecular Paleohydrology: Interpreting the Hydrogen-Isotopic Composition of Lipid Biomarkers from Photosynthesizing Organisms. Annu. Rev. Earth Planet. Sci. 40, 221–249. doi:10.1146/annurev-earth-042711-105535
Sachse, D., Kahmen, A., Gleixner, G., 2009. Significant seasonal variation in the hydrogen isotopic composition of leaf-wax lipids for two deciduous tree ecosystems (Fagus sylvativa and Acer pseudoplatanus). Org. Geochem. 40, 732–742. doi:10.1016/j.orggeochem.2009.02.008
Sachse, D., Radke, J., Gleixner, G., 2006. δD values of individual *n*-alkanes from terrestrial plants along a climatic gradient – Implications for the sedimentary biomarker record. Org. Geochem. 37, 469–483. doi:10.1016/j.orggeochem.2005.12.003
Sachse, D., Radke, J., Gleixner, G., 2004. Hydrogen isotope ratios of recent lacustrine sedimentary *n*-alkanes record modern climate variability. Geochim. Cosmochim. Acta 68, 4877–4889. doi:10.1016/j.gca.2004.06.004

Scheffler, K., Hoernes, S., Schwark, L., 2003. Global changes during Carboniferous–Permian glaciation of Gondwana: Linking polar and equatorial climate evolution by geochemical proxies. Geology 31, 605–608. doi:10.1130/0091-7613(2003)031<0605:GCDCGO>2.0.CO;2

Schimmelmann, A., Lewan, M.D., Wintsch, R.P., 1999. D/H isotope ratios of kerogen, bitumen, oil, and water in hydrous pyrolysis of source rocks containing kerogen types I, II, IIS, and III. Geochim. Cosmochim. Acta 63, 3751–3766. doi:10.1016/S0016-7037(99)00221-5

Schimmelmann, A., Sessions, A.L., Mastalerz, M., 2006. Hydrogen Isotopic (D/H) Composition of Organic Matter During Diagenesis and Thermal Maturation. Annu. Rev. Earth Planet. Sci. 34, 501–533. doi:10.1146/annurev.earth.34.031405.125011

Schnyder, J., Pons, D., Yans, J., Tramoy, R., Abdulanova, S., accepted. Refined stratigraphy of a continental Pliensbachian-Toarcian Boundary section in Central Asia using palynology and carbon isotopes stratigraphy: Taskomirsay, SW Kazakhstan. In: Geological Evolution of Central Asia and the Tien Shan Range. Eds M-F Brunet, T. McCann, E.R. Sobel, volume n° 427 Special Publications, Geological Society of London.

Schouten, S., Hopmans, E.C., Sinninghe Damsté, J.S., 2013. The organic geochemistry of glycerol dialkyl glycerol tetraether lipids: A review. Org. Geochem. 54, 19–61. doi:10.1016/j.orggeochem.2012.09.006

Schubert, C.J., Calvert, S.E., 2001. Nitrogen and carbon isotopic composition of marine and terrestrial organic matter in Arctic Ocean sediments: implications for nutrient utilization and organic matter composition. Deep Sea Res. Part Oceanogr. Res. Pap. 48, 789–810. doi:10.1016/S0967-0637(00)00069-8

Schulz, E., 1967. Sporenpaläontologisce Untersuchungen rätoliassischer Schichten im Zentralteil des germanischen Beckens. Palaeontol. Abh. Abt. B Paläobotanik 2, 541–633.

Sessions, A.L., 2016. Factors controlling the deuterium contents of sedimentary hydrocarbons. Org. Geochem. 96, 43–64. doi:10.1016/j.orggeochem.2016.02.012

Sessions, A.L., Burgoyne, T.W., Schimmelmann, A., Hayes, J.M., 1999. Fractionation of hydrogen isotopes in lipid biosynthesis. Org. Geochem. 30, 1193–1200. doi:10.1016/S0146-6380(99)00094-7

Sessions, A.L., Sylva, S.P., Summons, R.E., Hayes, J.M., 2004. Isotopic exchange of carbon-bound hydrogen over geologic timescales. Geochim. Cosmochim. Acta 68, 1545–1559. doi:10.1016/j.gca.2003.06.004

Shaw, A.J., Devos, N., Cox, C.J., Boles, S.B., Shaw, B., Buchanan, A.M., Cave, L., Seppelt, R., 2010. Peatmoss (Sphagnum) diversification associated with Miocene Northern Hemisphere climatic cooling? Mol. Phylogenet. Evol. 55, 1139–1145. doi:10.1016/j.ympev.2010.01.020

Shepherd, T., Wynne Griffiths, D., 2006. The effects of stress on plant cuticular waxes. New Phytol. 171, 469–499. doi:10.1111/j.1469-8137.2006.01826.x

Silva, J.A., Bremner, J.M., 1966. Determination and Isotope-Ratio Analysis of Different Forms of Nitrogen in Soils: 5. Fixed Ammonium1. Soil Sci. Soc. Am. J. 30, 587. doi:10.2136/sssaj1966.03615995003000050017x

Smith, F.A., Freeman, K.H., 2006. Influence of physiology and climate on δD of leaf wax *n*-alkanes from C_3 and C_4 grasses. Geochim. Cosmochim. Acta 70, 1172–1187. doi:10.1016/j.gca.2005.11.006

Smith, F.A., Wing, S.L., Freeman, K.H., 2007. Magnitude of the carbon isotope excursion at the Paleocene–Eocene thermal maximum: The role of plant community change. Earth Planet. Sci. Lett. 262, 50–65. doi:10.1016/j.epsl.2007.07.021

Sobel, E.R., 1999. Basin analysis of the Jurassic–Lower Cretaceous southwest Tarim basin, northwest China. Geol. Soc. Am. Bull. 111, 709–724. doi:10.1130/0016-7606(1999)111<0709:BAOTJL>2.3.CO;2

Stefanova, M., Ivanov, D.A., Simoneit, B.R.T., 2013. Paleoenvironmental application of *Taxodium* macrofossil biomarkers from the Bobov dol coal formation, Bulgaria. Int. J. Coal Geol. 120, 102–110. doi:10.1016/j.coal.2013.10.005

Storme, J.-Y., Dupuis, C., Schnyder, J., Quesnel, F., Garel, S., Iakovleva, A.I., Iacumin, P., Di Matteo, A., Sebilo, M., Yans, J., 2012. Cycles of humid-dry climate conditions around the P/E boundary: new stable isotope data from terrestrial organic matter in Vasterival section (NW France). Terra Nova 24, 114–122. doi:10.1111/j.1365-3121.2011.01044.x

Street, J.H., Anderson, R.S., Rosenbauer, R.J., Paytan, A., 2013. *n*-Alkane evidence for the onset of wetter conditions in the Sierra Nevada, California (USA) at the mid-late Holocene transition, ~ 3.0 ka. Quat. Res. 79, 14–23. doi:10.1016/j.yqres.2012.09.004

Suan, G., Mattioli, E., Pittet, B., Lécuyer, C., Suchéras-Marx, B., Duarte, L.V., Philippe, M., Reggiani, L., Martineau, F., 2010. Secular environmental precursors to Early Toarcian (Jurassic) extreme climate changes. Earth Planet. Sci. Lett. 290, 448–458. doi:10.1016/j.epsl.2009.12.047

Suan, G., Nikitenko, B.L., Rogov, M.A., Baudin, F., Spangenberg, J.E., Knyazev, V.G., Glinskikh, L.A., Goryacheva, A.A., Adatte, T., Riding, J.B., Föllmi, K.B., Pittet, B., Mattioli, E., Lécuyer, C., 2011. Polar record of Early Jurassic massive carbon injection. Earth Planet. Sci. Lett. 312, 102–113. doi:10.1016/j.epsl.2011.09.050

Swap, R.J., Aranibar, J.N., Dowty, P.R., Gilhooly III, W.P., Macko, S.A., 2004. Natural abundance of ^{13}C and ^{15}N in C_3 and C_4 vegetation of southern Africa: patterns and implications. Glob. Change Biol. 10, 350–358. doi:10.1111/j.1365-2486.2003.00702.x

Szpak, P., 2014. Complexities of nitrogen isotope biogeochemistry in plant-soil systems: implications for the study of ancient agricultural and animal management practices. Front. Plant Sci. 5. doi:10.3389/fpls.2014.00288

Thomas, B.A., 1972. A Probable Moss from the Lower Carboniferous of the Forest of Dean, Gloucestershire. Ann. Bot. 36, 155–161.

Tramoy, R., Salpin, M., Schnyder, J., Person, A., Sebilo, M., Yans, J., Vaury, V., Fozzani, J., Bauer, H., 2016. Stepwise palaeoclimate change across the Eocene–Oligocene transition recorded in continental NW Europe by mineralogical assemblages and $\delta^{15}N_{org}$ (Rennes Basin, France). Terra Nova 28, 212–220. doi:10.1111/ter.12212

Tyson, R.V., 1995. Sedimentary Organic Matter, Chapman and Hall. ed.

Vakhrameev, V.A., 1991. Jurassic and Cretaceous Floras and Climates of the Earth. Cambridge University Press.

van de Schootbrugge, B., Bailey, T.R., Rosenthal, Y., Katz, M.E., Wright, J.D., Miller, K.G., Feist-Burkhardt, S., Falkowski, P.G., 2005. Early Jurassic climate change and the radiation of organic-walled phytoplankton in the Tethys Ocean. Paleobiology 31, 73–97. doi:10.1666/0094-8373(2005)031<0073:EJCCAT>2.0.CO;2

Wang, Y., Mosbrugger, V., Zhang, H., 2005. Early to Middle Jurassic vegetation and climatic events in the Qaidam Basin, Northwest China. Palaeogeogr. Palaeoclimatol. Palaeoecol., 224, 200–216. doi:10.1016/j.palaeo.2005.03.035

Warren, C.R., McGrath, J.F., Adams, M.A., 2001. Water availability and carbon isotope discrimination in conifers. Oecologia 127, 476–486. doi:10.1007/s004420000609

Weete, J.D., Leek, G.L., Peterson, C.M., Currie, H.E., Branch, W.D., 1978. Lipid and Surface Wax Synthesis in Water-stressed Cotton Leaves. Plant Physiol. 62, 675–677. doi:10.1104/pp.62.5.675

1253 Weijers, J.W.H., Schouten, S., van den Donker, J.C., Hopmans, E.C., Sinninghe Damsté, J.S.,
1254 2007. Environmental controls on bacterial tetraether membrane lipid distribution in
1255 soils. Geochim. Cosmochim. Acta 71, 703–713. doi:10.1016/j.gca.2006.10.003
1256 Yang, H., Huang, Y., 2003. Preservation of lipid hydrogen isotope ratios in Miocene
1257 lacustrine sediments and plant fossils at Clarkia, northern Idaho, USA. Org. Geochem.
1258 34, 413–423. doi:10.1016/S0146-6380(02)00212-7
1259

1260

Figure 1-revised

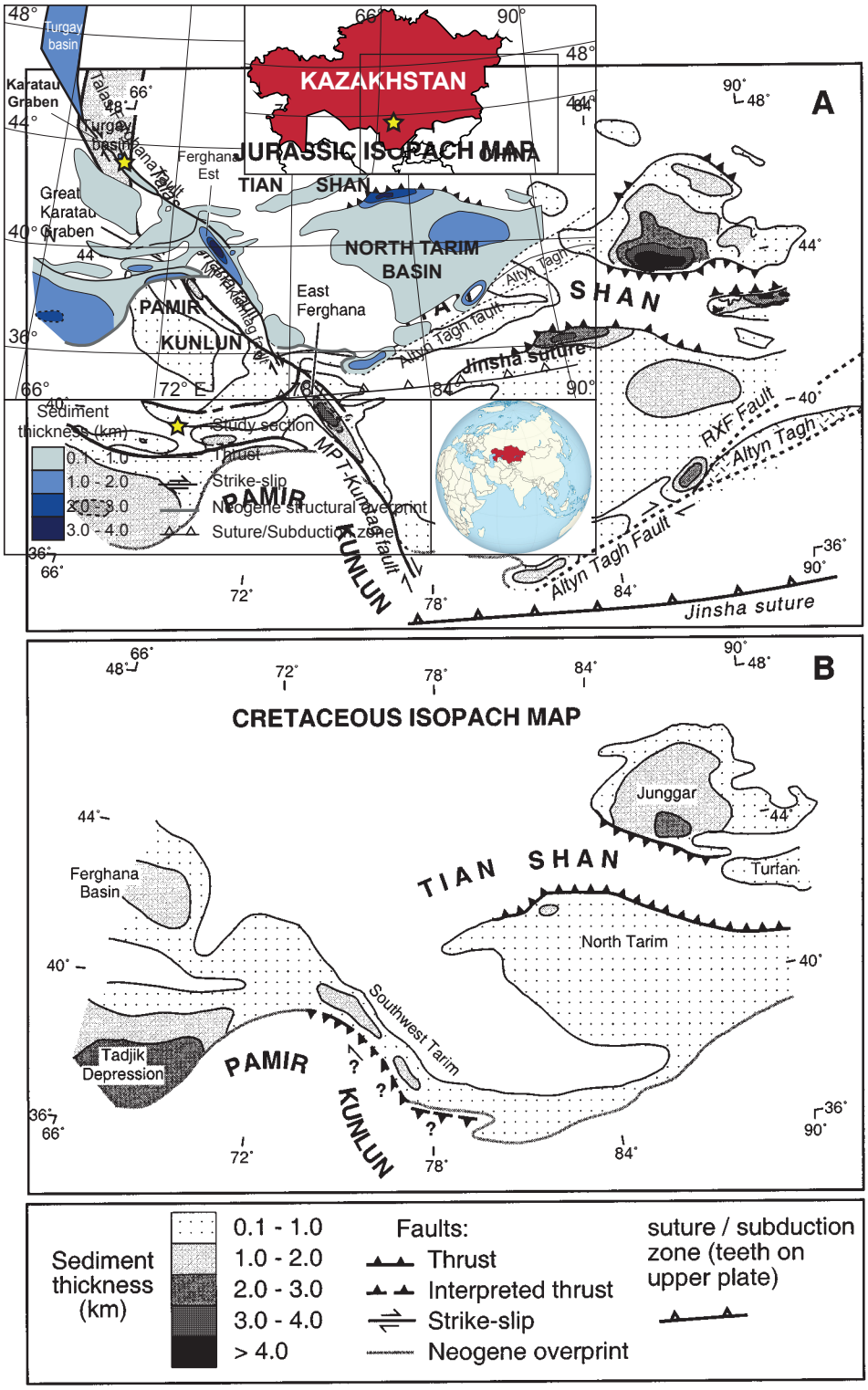

Figure 2-revised

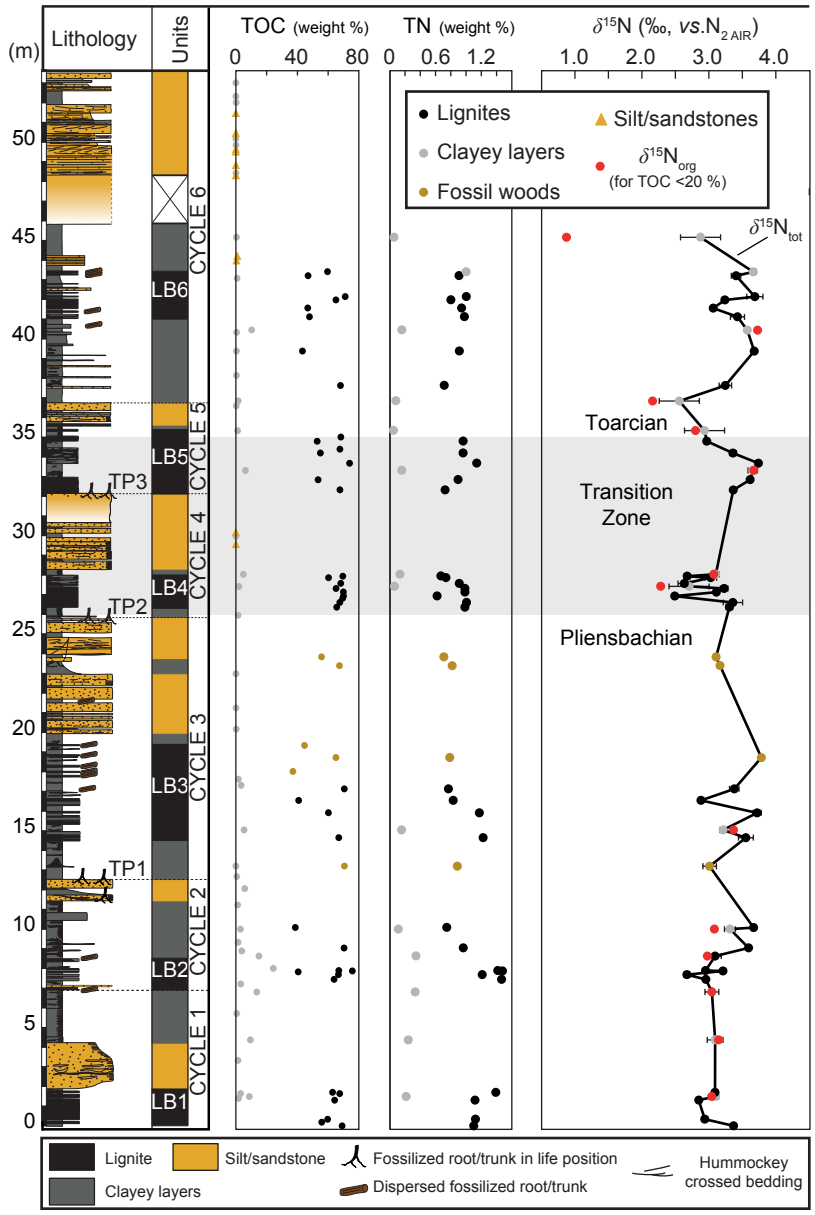

Figure 3

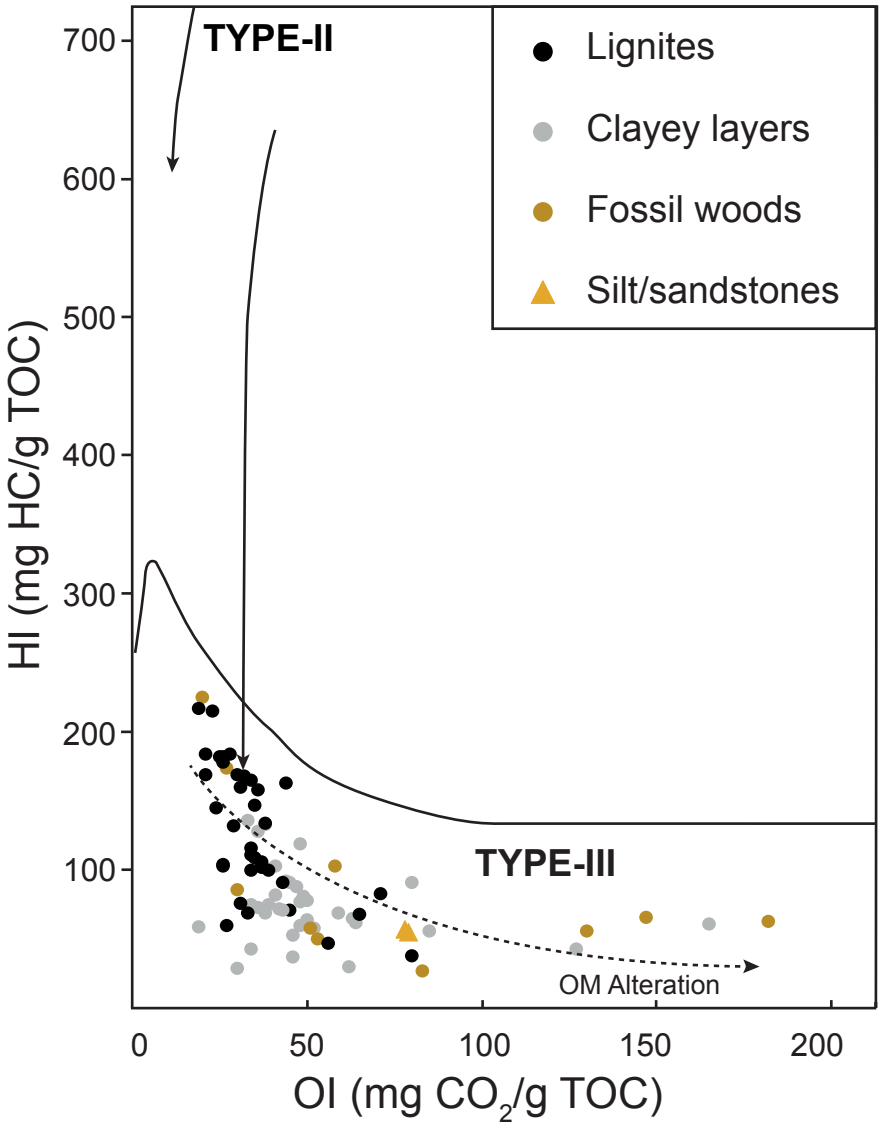
TYPE-II
TYPE-III
Lignites
Clayey layers
Fossil woods
Silt/sandstones
OM Alteration
HI (mg HC/g TOC)
OI (mg CO2/g TOC)
700
600
500
400
300
200
100
0
50
100
150
200

Figure 4-revised

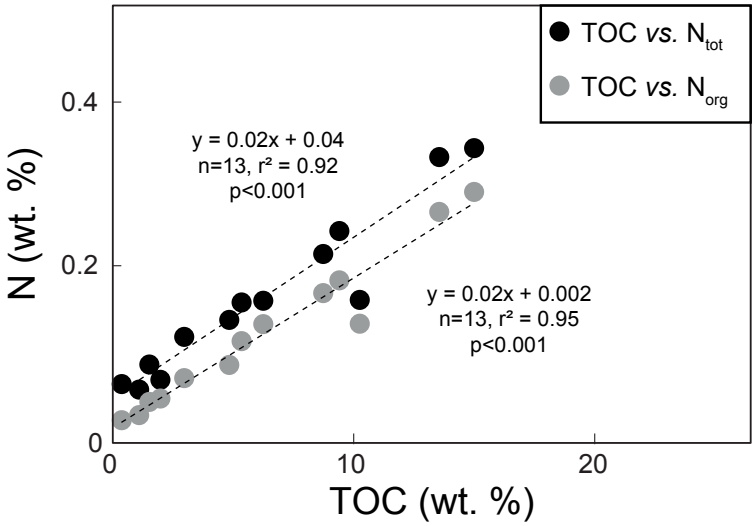

Figure 5-revised

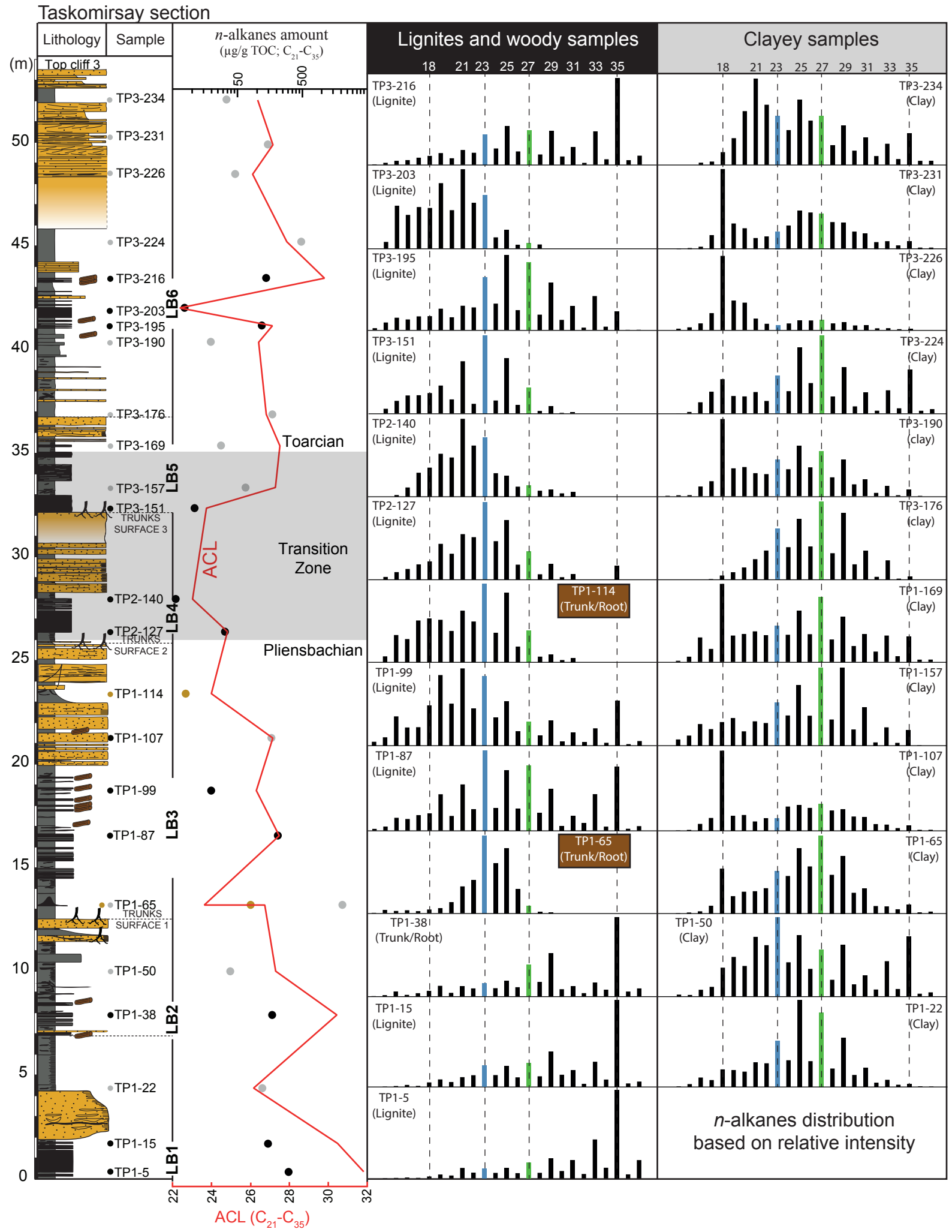

Figure 6-revised

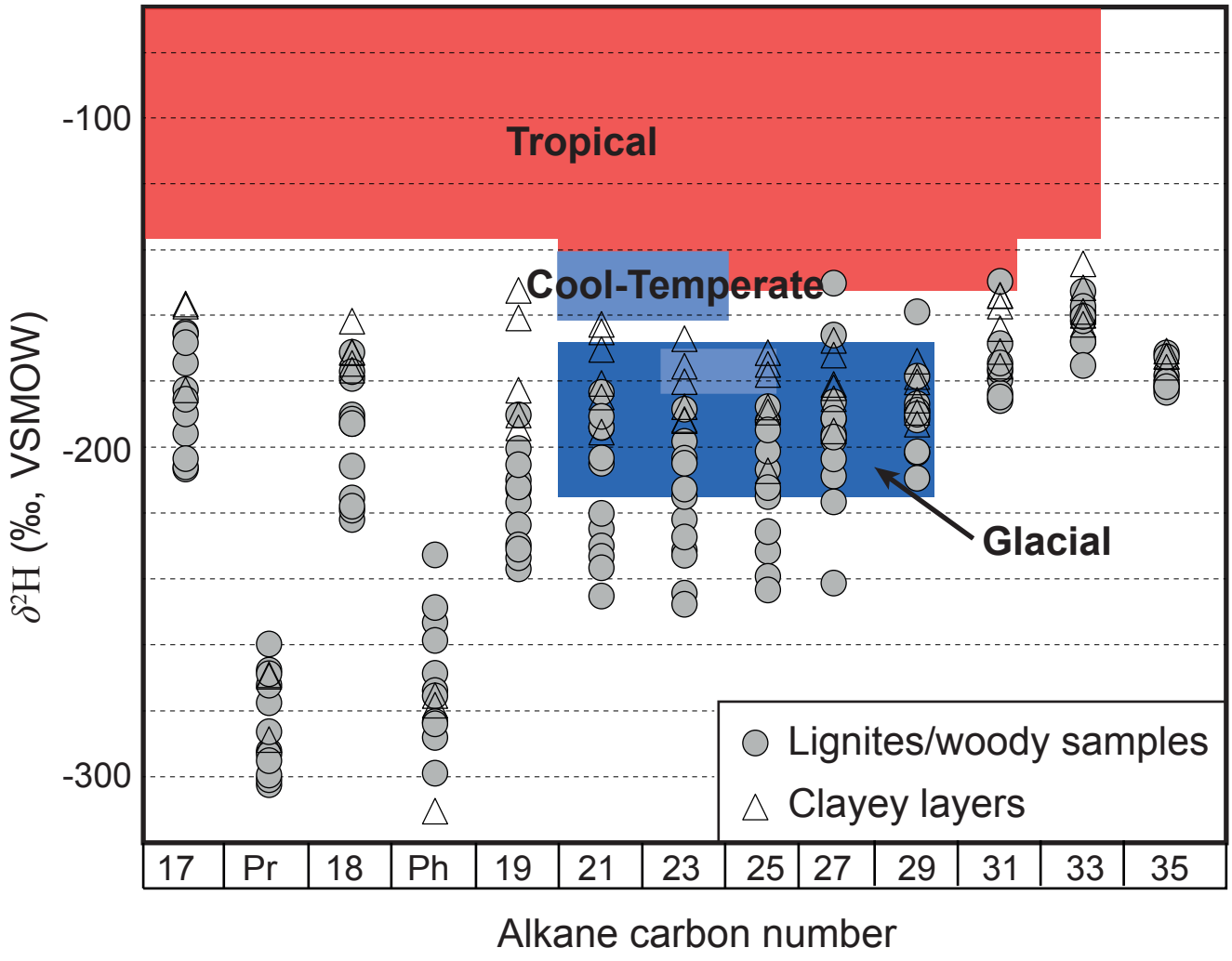

Figure 7-revised

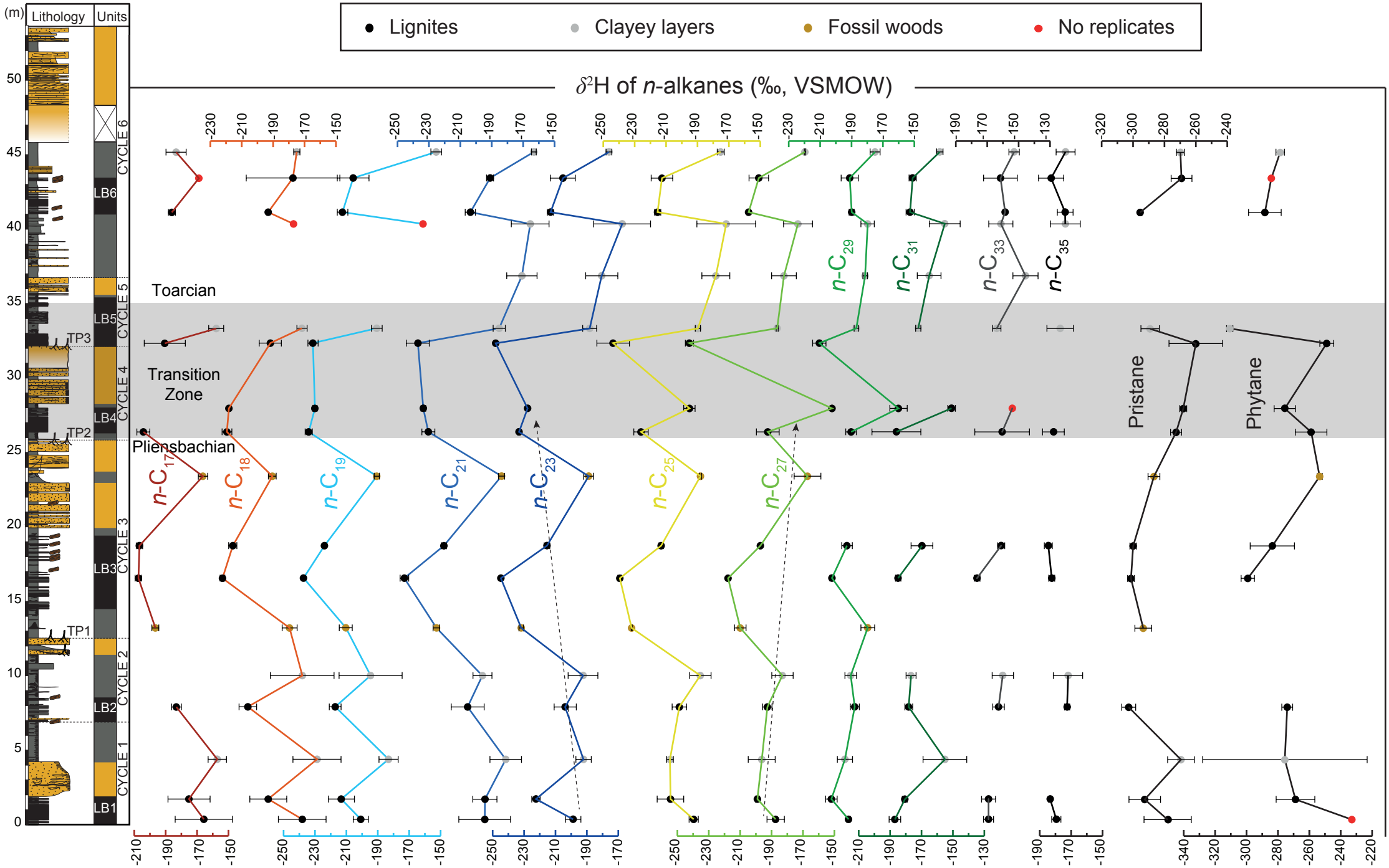

Figure 8

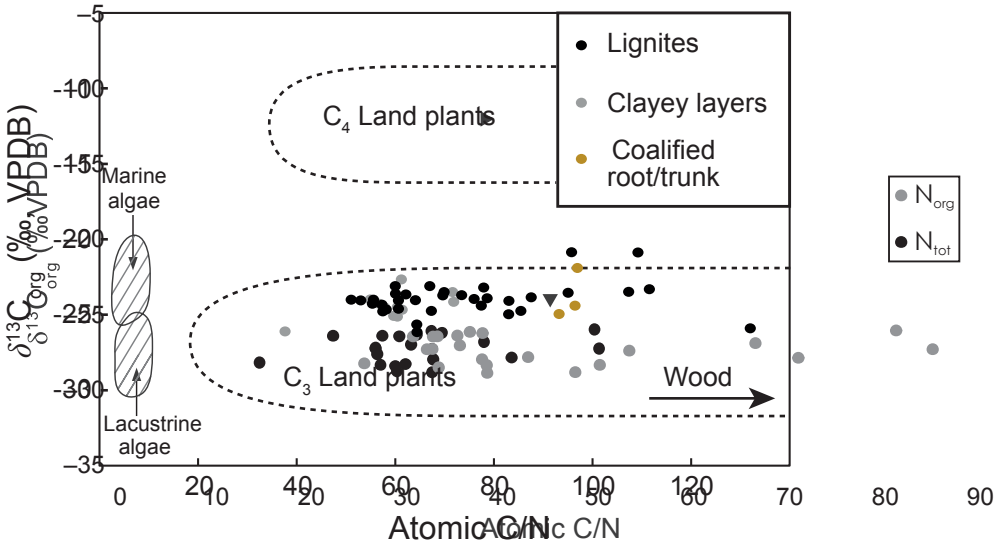
Lignites
Clayey layers
Coalified root/trunk
C4 Land plants
C3 Land plants
Wood
Marine algae
Lacustrine algae
Norg
Ntot
δ13Corg (‰ VPDB)
Atomic C/N
Atomic C/N

Figure 9-revised

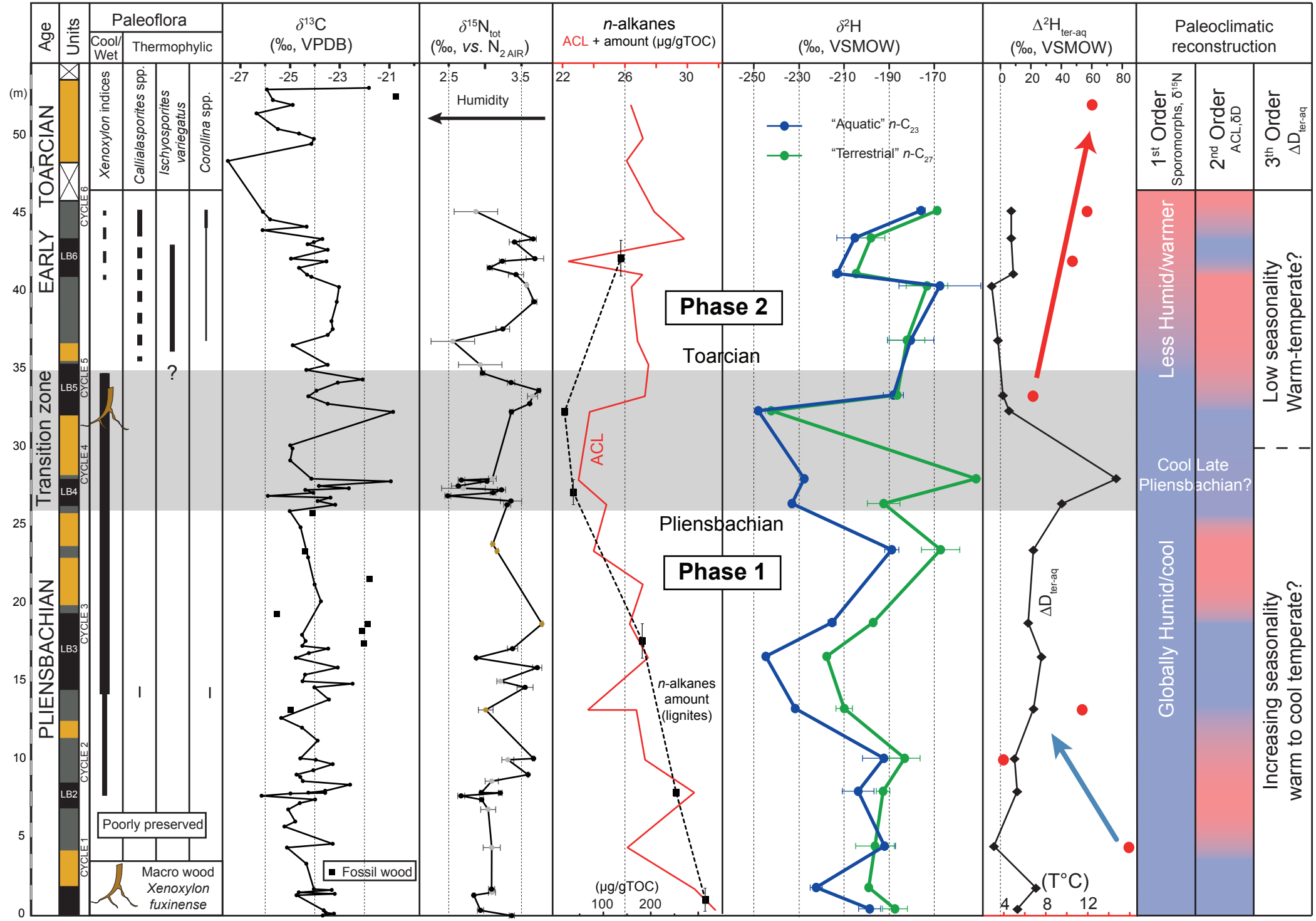

Figure 10

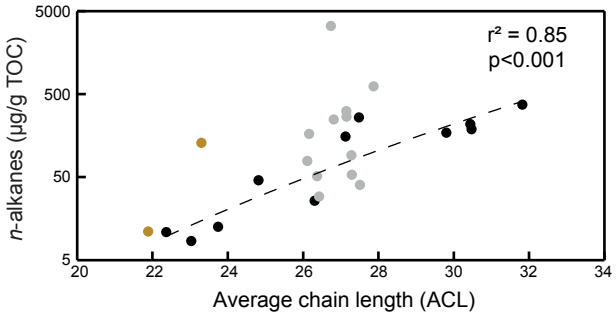
5000
500
50
5
n-alkanes (µg/g TOC)
r² = 0.85
p<0.001
20
22
24
26
28
30
32
34
Average chain length (ACL)

Table 1

Click here to download Table: Table 1.pdf

Table 1

Sample	Position (m)	Lithology	[a]TOC (%)	[b]TN (%)	[c]C/N	[d]N_{bnd} (%)	[e]N_{org} (%)	$\delta^{15}N$ (‰)		$\delta^{15}N_{org}$ (‰)
								mean	SD	
TP3-234	52.02	Clay	0.2	-	-	-	-	-	-	
TP3-231	49.85	Clay	0.1	-	-	-	-	-	-	
TP3-226	48.43	Clay	0.1	-	-	-	-	-	-	
TP3-224	45.17	Clay	0.4	0.06	*38	0.04	0.01	2.9	0.30	0.9
TP3-216	43.41	Lignite	59.6	1.00	70	-	0.24	3.7	0.04	
TP3-212	43.21	Lignite	47.0	0.91	61	-	0.53	3.4	0.07	
TP3-205	42.15	Lignite	71.2	1.00	83	-	0.16	3.7	0.12	
TP3-203	41.98	Lignite	65.1	0.80	95	-	0.13	3.2	0.04	
TP3-201	41.57	Lignite	46.8	0.94	58	-	0.38	3.1	0.04	
TP3-195	41.12	Lignite	47.9	0.98	57	-	0.42	3.4	0.11	
TP3-191	40.45	OM-rich Clay	10.3	0.16	*93	0.03	0.13	3.6	0.01	3.7
TP3-190	40.34	Clay	0.4	-	-	-	-	-	-	
TP3-185bis	39.38	Lignite	43.3	0.91	56	-	0.28	3.7	0.04	
TP3-179	37.63	Lignite	68.1	0.71	112	-	0.14	3.2	0.09	
TP3-176	36.85	Clay	1.5	0.08	*53	0.05	0.03	2.6	0.30	
TP3-169	35.34	Clay	1.1	0.05	*72	0.03	0.02	2.9	0.30	2.8
TP3-165	34.80	Lignite	52.9	0.96	64	-	0.38	3.0	0.03	3.7
TP3-162	34.20	Lignite	55.0	0.96	67	-	0.46	3.4	0.05	
TP3-159	33.68	Lignite	74.0	1.14	76	-	0.22	3.7	0.02	
TP3-157	33.32	OM-rich Clay	6.2	0.16	*57	0.03	0.13	3.7	0.07	3.7
TP3-153	32.84	Lignite	53.5	0.90	70	-	0.26	3.6	0.00	
TP3-151	32.32	Lignite	67.7	0.73	109	-	0.37	3.4	0.02	
TP2-141	28.03	Clay	4.8	0.13	*72	0.06	0.08	3.1	0.05	3.1
TP2-140	27.94	Lignite	69.6	0.67	121	-	0.09	2.7	0.05	
TP2-139	27.86	Lignite	60.3	0.74	96	-	0.15	3.0	0.09	
TP2-135	27.57	Lignite	68.2	0.91	88	-	0.18	2.6	0.09	
TP2-133	27.42	Clay	2.0	0.06	*61	0.02	0.04	2.7	0.30	2.3
TP2-132	27.31	Lignite	65.2	0.99	77	-	0.19	3.2	0.06	
TP2-131	27.13	Lignite	69.9	0.99	83	-	0.23	3.1	0.04	
TP2-130	26.93	Lignite	70.0	0.62	132	-	0.09	2.5	0.04	
TP2-128	26.60	Lignite	67.6	1.01	79	-	0.25	3.4	0.15	
TP1-127	26.36	Lignite	65.6	0.99	78	-	0.29	3.3	0.05	
TP1-117	23.84	Coalified root/trunk	55.7	0.71	92	-	0.16	3.1	0.02	
TP1-114	23.39	Coalified root/trunk	67.4	0.82	96	-	0.18	3.2	0.01	
TP3-107	21.24	Clay	0.1	-	-	-	-	-	-	
TP1-99	18.72	Coalified root/trunk	65.1	0.79	97	-	0.13	3.8	0.01	
TP1-89	17.13	Lignite	70.6	0.77	107	-	0.08	3.4	0.07	
TP1-87	16.54	Lignite	40.8	0.83	57	-	0.48	2.9	0.00	
TP1-84	15.91	Lignite	60.2	1.17	60	-	0.34	3.7	0.06	
TP1-76	15.04	Clay	5.3	0.16	*58	0.05	0.11	3.2	0.05	3.4
TP1-71	14.65	Lignite	67.0	1.22	64	-	0.26	3.6	0.11	
TP1-65	13.20	Coalified root/trunk	70.6	0.89	93	-	0.15	3.0	0.10	
TP3-65	13.20	Clay	0.02	-	-	-	-	-	-	
TP1-51	10.08	Lignite	38.7	0.75	61	-	0.42	3.7	0.01	
TP1-50	9.99	Clay	3.0	0.11	*55	0.05	0.06	3.3	0.08	3.1
TP1-46	9.04	Lignite	70.4	0.96	85	-	0.13	3.6	0.00	
TP1-43	8.63	OM-rich Clay	15.0	0.34	*60	0.05	0.29	3.1	0.09	3.0

TP1-38	7.89	Lignite	67.0	1.42	55	-	0.24	2.9	0.02	
TP1-38base	7.87	Lignite	75.8	1.48	60	-	0.31	3.2	0.03	
TP1-35	7.68	Lignite	66.7	1.21	64	-	0.19	2.7	0.05	
TP1-33	7.44	Lignite	63.9	1.47	51	-	0.37	3.0	0.03	
TP1-29	6.80	OM-rich Clay	13.6	0.33	*60	0.07	0.27	3.0	0.10	3.0
TP1-22	4.36	OM-rich Clay	9.4	0.24	*60	0.06	0.18	3.1	0.12	3.1
TP1-15	1.70	Lignite	62.9	1.39	53	-	0.32	3.1	0.04	
TP1-11	1.48	OM-rich Clay	8.7	0.21	*61	0.05	0.17	3.1	0.05	3.0
TP1-8	1.30	Lignite	64.3	1.12	67	-	0.38	2.8	0.01	
TP1-5	0.33	Lignite	59.7	1.12	62	-	0.29	2.9	0.04	
TP1-1	0.00	Lignite	69.1	1.10	73	-	0.56	3.4	0.04	
	Average			**0.77**			**0.23**	**3.2**		

Table 2

Click here to download Table: Table 2.pdf

Table 2.

Sample	Lithology	Position (m)	TOC (%)	[a] Lipid content (%)	*n*-alkane range (max; sub-maxs)	*n*-alkane content (µg/gTOC)	CPI (C_{21}-C_{35})	ACL (C_{21}-C_{35})	Pr/Ph ratio	[b] MAAT (°C)
TP3-234	Clay	52.02	0.2	0.01	C_{16}-C_{37} (C_{21}; C_{25}; C_{35})	51	1.7	26.4	0.3	12.4
TP3-231	Clay	49.85	0.1	<0.01	C_{14}-C_{37} (C_{23})	268	1.1	27.2	0.3	-
TP3-226	Clay	48.43	0.1	<0.01	C_{14}-C_{35} (C_{18}; C_{27})	78	1.1	26.1	0.3	-
TP3-224	Clay	45.17	0.6	0.13	C_{14}-C_{37} (C_{27}; C_{35}; C_{18})	621	3.2	27.9	0.7	11.9
TP3-216	Lignite	43.41	59.6	1.85	C_{13}-C_{37} (C_{35}; C_{25}; C_{29})	172	4.0	29.8	3.9	-
TP3-203	Lignite	41.98	65.1	0.86	C_{14}-C_{28} (C_{21})	11	2.0	22.4	2.0	10.5
TP3-195	Lignite	41.12	47.9	2.08	C_{13}-C_{37} (C_{23}; C_{33})	154	3.2	27.1	5.7	-
TP3-190	Clay	40.34	0.4	0.01	C_{13}-C_{36} (C_{18}; C_{25})	29	1.8	26.4	1.0	-
TP3-176	Clay	36.85	1.5	0.03	C_{17}-C_{35} (C_{27})	247	2.3	26.8	2.1	-
TP3-169	Clay	35.34	1.1	<0.01	C_{14}-C_{37} (C_{18}; C_{27})	40	2.1	27.5	0.8	-
TP3-157	OM-rich Clay	33.32	6.2	0.21	C_{14}-C_{36} (C_{29}; C_{27})	92	2.6	27.3	7.6	6.8
TP3-151	Lignite	32.32	73.1	2.49	C_{14}-C_{35} (C_{23})	13	5.5	23.7	2.7	-
TP2-140	Lignite	27.94	69.6	1.27	C_{15}-C_{31} (C_{21})	8	1.6	23.0	2.6	-
TP2-127	Lignite	26.36	65.6	2.06	C_{14}-C_{35} (C_{23})	46	2.1	24.8	6.7	-
TP1-114	Coalified root/trunk	23.39	67.4	3.64	C_{14}-C_{35} (C_{23}; C_{18})	11	2.3	24.0	6.0	-
TP1-107	Clay	21.24	0.1	<0.01	C_{14}-C_{37} (C_{18}; C_{27})	311	1.1	27.2	0.6	-
TP1-99	Coalified root/trunk	18.72	75.4	2.35	C_{13}-C_{37} (C_{21}; C_{35}; C_{29})	26	2.7	26.3	6.1	-
TP1-87	Lignite	16.54	38.6	1.90	C_{13}-C_{37} (C_{23}; C_{27}; C_{35})	262	3.8	27.5	3.3	-
TP1-65	Coalified root/trunk	13.20	70.6	2.23	C_{13}-C_{29} (C_{23})	129	1.6	23.6	1.7	11.5
TP1-65bis	Clay	13.20	0.02	<0.01	C_{14}-C_{37} (C_{27}; C_{18})	3313	1.6	26.7	0.9	-
TP1-50	Clay	10.00	3.0	0.1	C_{14}-C_{37} (C_{23}; C_{35}; C_{29})	53	2.4	27.3	3.2	4.0
TP1-38	Lignite	7.89	67.0	3.90	C_{11}-C_{37} (C_{35}; C_{29}; C_{19})	218	3.5	30.4	4.5	-
TP1-22	Clay	4.36	9.4	0.58	C_{14}-C_{37} (C_{25})	166	2.6	26.2	2.9	15.9
TP1-15	Lignite	1.70	62.9	2.65	C_{14}-C_{37} (C_{35}; C_{29}; C_{23})	189	3.4	30.5	6.6	-
TP1-5	Lignite	0.34	59.7	2.43	C_{14}-C_{37} (C_{35}; C_{29}; C_{23})	374	4.4	31.8	5.4	-
Average							**2.5**	**26.7**	**3.1**	

Table 3

Click here to download Table: Table 3.pdf

Table 3.

Sample	Lithology	C_{17}	SD (1σ)	C_{18}	SD (1σ)	C_{19}	SD (1σ)	C_{21}	SD (1σ)	C_{23}	SD (1σ)	C_{25}	SD (1σ)
TP3-224	Clay	−183	6	−175	2	−153	3	−163	2	−176	2	−175	2
TP3-216	Lignite	−169	-	−177	30	−206	10	−191	2	−205	8	−213	7
TP3-195	Lignite	−186	2	−193	1	−212	3	−204	3	−213	2	−215	2
TP3-190	Clay	-	-	−177	-	−161	-	−166	12	−168	18	−172	19
TP3-176	Clay	-	-	-	-	-	-	−171	10	−181	10	−178	9
TP3-157	OM-rich clay	−158	5	−172	3	−191	3	−185	4	−188	4	−190	2
TP3-151	Lignite	−190	13	−192	7	−231	3	−237	7	−248	1	−244	10
TP2-140	Lignite	-	-	−218	1	−230	1	−234	2	−228	<1	−195	4
TP2-127	Lignite	−204	4	−220	3	−234	2	−230	4	−233	1	−226	5
TP1-114	Coalified root/trunk	−166	3	−191	2	−191	2	−184	2	−189	3	−188	1
TP1-99	Coalified root/trunk	−206	2	−216	3	−224	1	−220	2	−215	2	−213	1
TP1-87	Lignite	−207	2	−222	2	−237	1	−246	3	−245	<1	−240	1
TP1-65	Coalified root/trunk	−196	2	−180	5	−210	4	−225	2	−232	1	−232	<1
TP1-50	Clay	-	-	−172	20	−195	20	−196	6	−192	9	−188	7
TP1-38	Lignite	−183	3	−206	6	−217	4	−205	11	−204	7	−202	5
TP1-22	Clay	−157	6	−162	15	−183	6	−181	10	−192	5	−208	2
TP1-15	Lignite	−175	13	−193	12	−213	8	−194	8	−222	3	−207	9
TP1-5	Lignite	−166	18	−172	15	−201	5	−194	16	−199	5	−193	3
	Average	**−182**	6	**−190**	8	**−205**	5	**−201**	6	**−207**	5	**−204**	5

Table 3. continued

Sample	C_{27}	SD (1σ)	C_{29}	SD (1σ)	C_{31}	SD (1σ)	C_{33}	SD (1σ)	C_{35}	SD (1σ)	Pr	SD (1σ)	Ph	SD (1σ)
TP3-224	−169	1	−175	3	−158	2	−153	3	−174	6	−270	3	−279	3
TP3-216	−198	6	−191	6	−176	2	−162	11	−183	8	−269	7	−284	-
TP3-195	−205	<1	−190	2	−177	3	−159	1	−174	5	−295	1	−288	10
TP3-190	−173	9	−180	4	−155	10	−161	8	−174	10	-	-	-	-
TP3-176	−182	8	−181	2	−165	8	−146	8	-	-	-	-	-	-
TP3-157	−187	1	−187	1	−172	2	−164	3	−177	9	−289	6	−311	2
TP3-151	−242	3	−211	4	-	-	-	-	-	-	−260	17	−249	4
TP2-140	−152	<1	−160	6	−151	3	−154	-	-	-	−268	2	−276	7
TP2-127	−192	7	−190	3	−186	16	−160	17	−181	7	−273	4	−259	10
TP1-114	−167	9	-	-	-	-	-	-	-	-	−287	4	−254	2
TP1-99	−197	1	−193	3	−170	7	−161	2	−185	3	−300	2	−284	14
TP1-87	−218	1	−203	1	−185	2	−176	2	−182	2	−301	2	−299	4
TP1-65	−210	4	−180	4	-	-	-	-	-	-	−294	5	-	-
TP1-50	−183	7	−191	4	−177	3	−160	7	−172	9	-	-	-	-
TP1-38	−193	3	−188	3	−178	3	−163	4	−173	2	−303	4	−274	3
TP1-22	−196	9	−194	5	−155	14	-	-	-	-	−269	9	−276	-
TP1-15	−199	1	−203	4	−181	2	−169	4	−183	1	−293	10	−269	12
TP1-5	−187	6	−192	1	−187	4	−169	3	−180	*3*	−278	15	−233	-
Average	**−192**	4	**−189**	3	**−172**	5	**−161**	6	**−178**	5	**−283**	6	**−274**	7

Figure Caption

Fig. 1. Geological and geographical situation of the Taskomirsay section (modified from Schnyder et al. accepted).

Fig. 2. Total organic carbon (TOC), Total Nitrogen (TN), $\delta^{15}N_{tot}$ and $\delta^{15}N_{org}$ values along the Taskomirsay section with respect to lithology. Lignites are in black, clayey layers in gray, silts-sandstones in orange triangles and coalified wood trunks or roots in brown. Transition zone, Pliensbachian-Toarcian transition.

Fig. 3. Taskomirsay samples plotted in a HI (Hydrogen Index)/OI (Oxygen Index) diagram. Arrows indicate pathways of OM alteration.

Fig. 4. TOC values of clayey layers plotted against corresponding N_{tot} and N_{org} values.

Fig. 5. ACL values, *n*-alkane amount and *n*-alkane distribution in lipid extracts of the Taskomirsay section. Blue bars refer to the "aquatic pool" (C_{23}) and green bars to the "terrestrial pool" (C_{27}) (see text, section 4.2).

Fig. **6**. Variability of $\delta^{2}H$ values of *n*-alkanes and isoprenoid pristane (Pr) and phytane (Ph). Also represented are compiled typical values under tropical, cool temperate and glacial regime from Dawson et al. (2004) and Izart et al. (2012).

Fig. 7. $\delta^{2}H$ values of *n*-alkanes and isoprenoid pristane and phytane along the Taskomirsay section. Error bars (based on triplicates) are smaller than the symbol if not visible, except for red points, which correspond to single analyses.

Fig. 8. Elemental atomic C/N ratio and organic isotopic values ($\delta^{13}C_{org}$) of bulk organic matter from Taskomirsay. Also represented are typical zones for different organic sources (modified from Meyers et al., 1997 with typical C/N values from Tyson, 1995).The $\delta^{13}C_{org}$ values are from Schnyder et al., accepted.

Fig. 9. Synthesized paleoclimatic parameters in Taskomirsay. Sporomorphs data and the $\delta^{13}C_{org}$ curve are from Schnyder et al., accepted. Temperatures (large red points) are based on brGDGTs and arrows show a cooling

trend (blue) and a warming trend (red). $\Delta^2H_{ter\text{-}aq}$ values were calculated as follows: mean δ^2H-C_{27} value minus mean δ^2H-C_{23} value.

Fig. 10. ACL values *vs. n*-alkane amounts. Significant logarithmic correlation occurs in lignites (black points). See Fig. 2 for color caption.

Table Caption

Table 1. Bulk organic results. Isotopic values are reported with their standard deviation (1σ) calculated on replicates analyses (2 at least). Standard deviation calculated on tyrosines (±0.3‰) was applied for samples below 40 µg N (highlighted in grey).

[a] total organic carbon

[b] total nitrogen

[c] atomic C/N ratio

[d] inorganic bound nitrogen

[e] organic nitrogen calculated by $TN - N_{bnd}$.

* TOC/N_{org} for clayey samples.

Table 2. Molecular geochemistry of the lipid extracts. *Relative abundances of brGDGTs used for MAAT calculations are in supplementary data.*

[a]*Percentage of lipids in dry sediments*

[b]*brGDGT-derived temperatures calculated from Peterse et al. (*2012)

Table 3. Hydrogen isotopes (δ^{2}H) of* n-*alkanes. *δ^2H values and their standard deviation (SD) are expressed in per mille (‰) from C_{17} to C_{35} and of pristane and phytane.*

Schnyder et al. text- Final revised paper

Click here to download Supplementary Interactive Plot Data (CSV): Schnyder-Cent-As-Bas-Revision 2.docx